

Micromachined Mechanical Resonant Sensors: From Materials, Structural Designs to Applications

Toan Dinh,* Mina Rais-Zadeh,* Thanh Nguyen, Hoang-Phuong Phan, Pingan Song, Ravinesh Deo, Dzung Dao, Nam-Trung Nguyen, and John Bell

Driving a micro and nanomechanical structure to resonance and observing its resonant motion in the physical world have led to numerous fundamental discoveries in physics, sciences, chemistry, biology, and engineering, as well as device commercialization. Scaling down mechanical structures from micrometric to nanometric size has enabled the utilization of resonant motions to probe material properties and various dynamical phenomena in quantum coherence and squeezing. Recent advances in material sciences and nanofabrication resulted in successful demonstration of ultra-high frequency operation (GHz range) and ultra-high quality factor (10 billion) micromachined mechanical resonators (MMRs). The resonant motion of these structures has been utilized as an indispensable tool to weigh biological and chemical species at resolution of atomic mass unit, sense a force as small as zepto-newton, and to detect numerous other physical parameters. Here, a systematic view on the resonant sensing transduction is provided, underlying physics, and sensing structures realized with micro/nano-electromechanical systems (MEMS/NEMS) technologies. It is also describe the roles of nanomaterials and structures, nano-fabrication and rational designs on the resonance frequency and quality factor of MMRs toward high-performance sensing. This paper discusses the most recent advances in the development of MMRs for material characterization as well as biological, chemical, and physical sensing. Finally, the paper discusses the challenges and perspectives on design, fabrication, and developments of resonant sensors with high quality factor toward quantum sensing, and ultra-high sensitivity and resolution for classical sensing applications.

1. Introduction

Micromachined mechanical resonators (MMRs) are mechanical structures fabricated by micromachining techniques, which are designed to vibrate freely at resonance. These devices operate under a wide range of modes and frequencies, ranging from several Hz to several GHz.^[1,2] The resonant frequency of resonators is determined a combination of intrinsic factors, such as material compositions and structural dimensions, as well as extrinsic parameters including engineering stress, environment temperature, density of surrounding environment.^[3,4] Extrinsic factors can also cause a decrease in amplitude of motion in resonators due to damping effects^[5] The quality factor, or Q , is a measure of the ratio of the energy stored to the energy lost in one cycle of vibration, and it is used to quantify the effects of damping.^[6,7] The changes in both Q and resonant frequency are commonly utilized as the sensing parameters to detect physical and biological inputs.^[8] In general, a high Q is desirable for sensing applications and studying physical interactions at the quantum level.^[9–14]

T. Dinh, T. Nguyen, P. Song, R. Deo, J. Bell
University of Southern Queensland
Springfield Central, Queensland 4300, Australia
E-mail: toan.dinh@usq.edu.au
M. Rais-Zadeh
Jet Propulsion Laboratory
NASA
CA 91109, USA
E-mail: Mina.rais-zadeh@jpl.nasa.gov

H.-P. Phan
University of New South Wales Sydney
Sydney, NSW 2052, Australia
D. Dao, N.-T. Nguyen
Griffith University
Nathan, Queensland 4111, Australia

 The ORCID identification number(s) for the author(s) of this article can be found under <https://doi.org/10.1002/admt.202300913>

© 2023 The Authors. Advanced Materials Technologies published by Wiley-VCH GmbH. This is an open access article under the terms of the [Creative Commons Attribution-NonCommercial License](#), which permits use, distribution and reproduction in any medium, provided the original work is properly cited and is not used for commercial purposes.

DOI: 10.1002/admt.202300913

The MMR sensing technology offers several benefits over conventional non-resonant sensing methods, including ultra-high sensitivity to external perturbations due to its miniaturization capability, and low noise or drift because of the high intrinsic Q factors.^[15–17] In addition, MRR sensors typically output the resonant frequency, which can be measured with a high degree of accuracy and easily converted into a digital signal.^[18] Thanks to their miniaturization and integration capabilities, MMR sensors can provide highly compact sensing solutions, such as lab-on-a-chip devices, which consume minimal energy.

The MMRs are the core component of resonant sensors that have found useful applications, ranging from probing material properties, a better understanding fundamental science and physics to device applications.^[19–23] In respect to their practical applications, MMRs and resonant sensors are usually found in timing references, atomic force microscopy (AFMs), accelerometers and mass sensing devices.^[24] In the areas of chemical and biological applications, micromachined resonators are for use in monitoring small molecules, and this aspect has attracted massive attention over the past decades especially in healthcare, food and environmental safety, and biosecurity.^[25] MRRs are capable of label-free detection of cells and biological molecules at an unprecedented high sensitivity and single molecule resolution, which has led to their use as a lab-on-a-chip resonant biosensing device.^[26] Examples of biosensing applications include early detection of various diseases, such as cancer cells. MMRs have been used to weigh polymer receptors and biomolecules at micro, nanoscale, and even single molecule levels.^[27] Resonant sensors have been shown to be effective tools for measuring temperature, thermal infrared radiation, force, stress and strain, pressure, and acceleration.^[28–32]

We now summarize the development of micromachined resonant sensors fabricated by MEMS/NEMS technologies.^[33–35] Some review papers have highlighted the importance of MMRs for biological and chemical detection purposes.^[3,36,37] More recently, nanomechanical resonators based on 1D (nanowire and nanotubes) and 2D materials (graphene and phosphorene) with low mass and wide frequency tuning have also been studied.^[38,39] In this review, we provide the most recent advances in the development of micromachined mechanical resonant sensors toward high-performance sensing applications. We will discuss the fundamental resonant sensing mechanism and the desired characteristics of resonant sensors (Section 2). We then provide updates on achieving high-frequency tuning and high-quality factor to realize ultra-high sensitivity. In Section 3 we also discuss recent efforts to scale down MMR to nanometric/atomic size using new materials and fabrication technologies. In Section 4, we will discuss recent successes in designing new MMR structures to address major challenges in reducing energy dissipation and taking advantage of strain engineering. In Section 5, we cover recent advances in applications of the MMRs sensor technology. Finally, we will provide perspectives on the development of MMR sensors in Section 6. **Figure 1** shows the overall MMR sensors and their representative applications in this review article.

2. Fundamentals of Micro-Machined Resonant Sensors

This section provides a fundamental understanding of sensing mechanism based on mechanical resonance. The two key parameters, namely resonance frequency and quality factors, as well as factors that influence these parameters, are discussed.

2.1. Resonant Sensing Mechanism

The mechanical motion of a structure in a linear regime can be described by a second order differential equation representing a mass-spring model as follow:

$$m\ddot{x} + b\dot{x} + kx = f_{\text{drive}} + f_{\text{th}} \quad (1)$$

where m , k and b are the mass, stiffness and damping coefficient, respectively; f_{drive} and f_{th} are the driving force and the thermomechanical noise force. The quality factor $Q = \sqrt{km}/b$ increases with increasing the effective mass and stiffness and reduced damping coefficient. The resonant frequency is given as: $f = \frac{1}{2\pi} \sqrt{\frac{k}{m}}$. The working principle of the mechanical resonant sensor is based on the change of the resonance frequency as a functional of measurands: physical or chemical inputs. **Figure 2** shows a representative mechanical structure that vibrates at resonance, showcasing how the resonance frequency shifts due to laser-induced temperature changes. There are two main resonance parameters, namely resonance frequency and quality factor.

2.1.1. MRR Sensors Based on Resonant Frequency

Changes in spring stiffness are induced by physical signals such as temperature (softening or hardening), force/strain and pressure. The effective mass of MMR sensors is widely utilized to quantify additional mass binding to the resonance structure, leading to a change in resonance frequency. An example of well-known mass sensor includes the detection of biological cells or chemical absorption on the MMR structure. The sensitivity of MMR sensors can be determined as: $S = \frac{\Delta f}{\Delta M}$, where Δf is the change of the resonance frequency due to the change of measurand ΔM . ΔM refers to changes in measurands, such as mass, temperature, and acceleration. Depending on the type of sensor, ΔM can represent Δm (mass change), ΔT (temperature change), or Δg (acceleration change) for mass sensors, temperature sensors, and accelerometers, respectively.

2.1.2. MRR Sensors Based on Quality Factor

The quality factor is a measure of the energy decay rate in a vibration cycle. A higher Q indicates a lower level of energy dissipation into the surrounding environment. Q is associated with the damping effect, and changes in damping can occur due to variations in the viscosity and density of the surrounding fluid. Therefore, MMR structures based on Q can be utilized as pressure sensors, vacuum sensors, and viscometers. Q can be

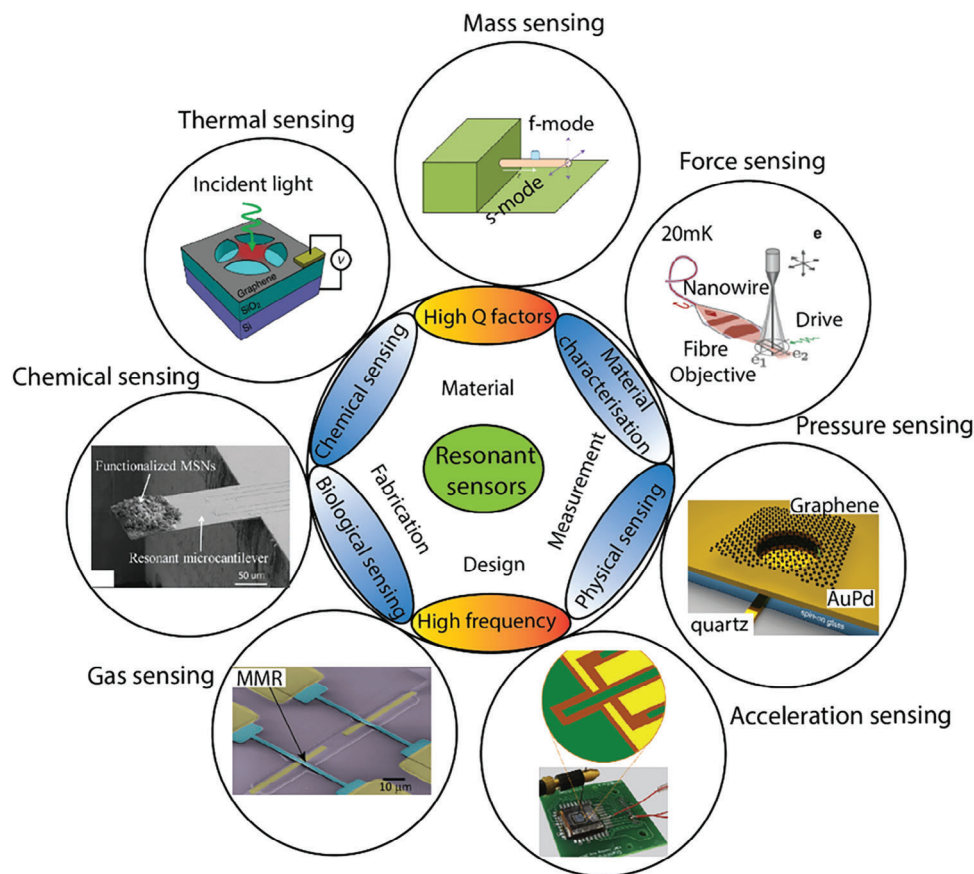


Figure 1. An overview on MMR sensors. Materials, designs, fabrication, and measurements of MMR sensors to achieve high frequency operation and high-quality factors for material/dynamical characterization and physical, chemical and biological sensing. Adapted with permission.^[40] Copyright 2021, Springer Nature – Force sensing;^[41] Copyright 2010, Springer Nature – Mass sensing;^[42] Copyright 2019, Springer Nature - Thermal sensing;^[43] Copyright 2018, Elsevier - Chemical sensing;^[44] Copyright 2012, Royal Society of Chemistry– Gas sensing;^[45] Copyright 2020, Elsevier– Acceleration sensing;^[46] Copyright 2017, American Chemical Society – Pressure sensing.

determined by the resonance frequency and frequency bandwidth B at 3 dB as $Q = \frac{f}{\Delta f}$. A high Q is crucial for sensing applications, as it lowers not only energy leakage and energy consumption to maintain resonance, but also signifies frequency

peak (resulting in a more precise determination of resonance frequency) and lower level of noise or a higher signal-to-noise ratio. A high Q allows the retention of energy for prolonged resonance and facilitates the detection of a small frequency change caused by perturbations. Improving Q plays the key role for achieving high-performance sensors and other devices. Since both high frequency and high Q are preferable for sensing applications, a high figure of merit $FM = f \times Q$ is desirable for MMR resonators and sensors.

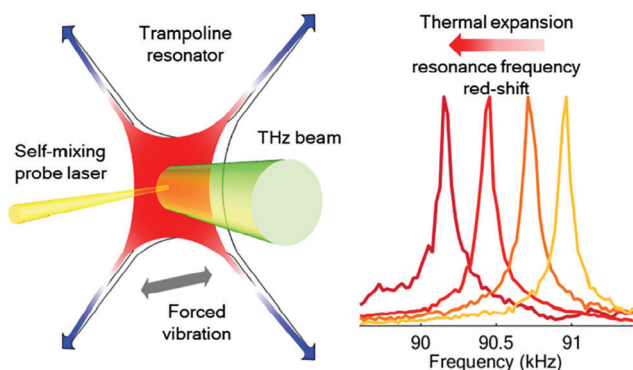


Figure 2. A trampoline membrane resonance structure exhibits a shift in the resonance frequency when subjected to laser-induced temperature changes. Reproduced with permission. Copyright 2022, American Chemical Society.^[47]

2.2. Actuation and Detection in MMR Sensors

In the operation of MMR sensors, external forces are required to actuate or drive them into vibration at their resonance frequency. To sense the vibration of these resonant sensors, various techniques are employed, including the detection of electrical and optical signals. **Figure 3** summarizes the actuation and detection methods for mechanical resonators and MMR sensors. The fundamentals of actuation and detection methods are provided as follows:

The actuation methods include: 1) Brownian motion harnesses the thermomechanical effect induced random thermal

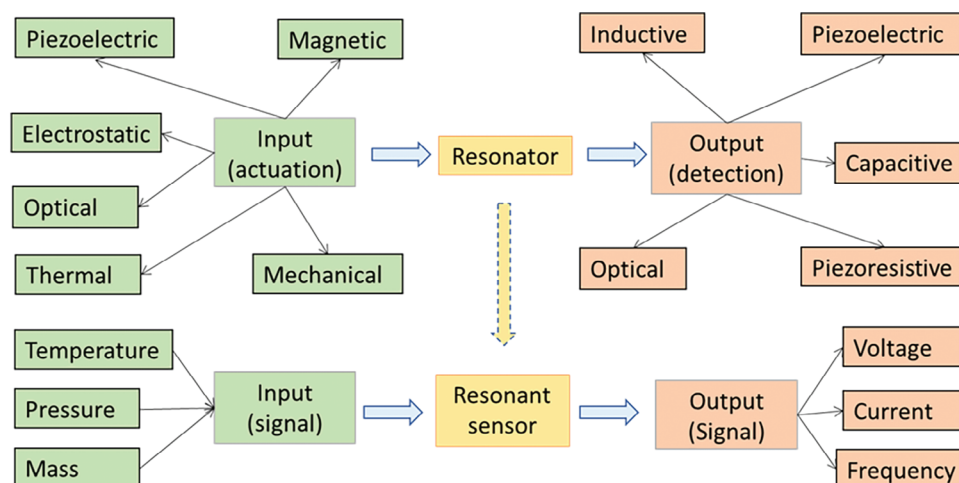


Figure 3. Actuation and sensing in resonators and resonant sensors. The actuation of mechanical resonance motion includes thermal, mechanical, electrostatic, magnetic and piezoelectric approaches; detection of mechanical resonance is based on piezoresistive, capacitive, inductive, piezoelectric and optical methods. Resonance sensors detect temperature, pressure and mass; the signals from resonance sensors are voltage, current, and frequency.

fluctuation. This method can be utilized for high-frequency resonators to enable sensing with high-order and multimodalities.^[48] 2) Mechanical actuation utilizes external mechanical forces or displacement to excite the MMR. For example, a constant applied force results in displacement, and upon releasing the force, the mechanical structures vibrate. Alternatively, a piezoelectric actuator, such as a shaker, drives MMR to resonance by applying an AC voltage. This method is widely used in conventional resonant sensors. However, its practical application is limited by the bulky supporting system that is typically required. 3) Electrothermal and optothermal actuations are based on the periodic thermal expansion induced by Joule heating (electrothermal) and laser-induced heating (optothermal), respectively. To achieve temperature rise through Joule heating, MMR sensors require materials with high electrical conductivity and low heat capacity. However, the thermal response of these materials is relatively slow, which poses a challenge for devices and sensors operating at high frequencies. The response time of thermal actuator is calculated as $\tau_{th} = R_{th}C_{th}$, where R_{th} and C_{th} are the thermal resistance and thermal capacitance.^[49] Large thermal resistance and capacitance cause a time delay for the temperature of the actuator to raise and generate force.^[49] Therefore, thermally actuated actuators typically work at low frequencies (e.g., MHz range).^[49] However, the time response of thermal actuator can be improved by scaling down the dimensions of the actuators.^[50] Optothermal actuation involves a periodic application of a short wavelength laser to locally heat up materials. This optothermal method became popular due to its precision and versatility. **Figure 4** shows a blue laser which is utilized to actuate the cantilever to resonance. The blue laser is located at the fixed end of the cantilever to enable the periodic thermal expansion to induce the thermal stress. 4) Electrostatic actuation or capacitive actuation relies on the generation of electrostatic forces between two parallel electrodes when a voltage is applied. This method is characterized by low power consumption, simplicity in design and suitable for practical applications. However, it would require high-voltage operation. 5) Piezoelectric actuation induces stress and strain in piezoelectric material when an AC voltage is applied. This method typ-

ically offers high precision control and fast response time. However, piezoelectric actuator requires integration of piezoelectric layers onto the resonators that can introduce complexity into the fabrication processes. Since this method does not require external bulky system support, it is suitable for on-chip actuation and practical applications. 6) Magnetic actuation is based on the magnetic force generated by the interaction between an electric current and a magnetic field. The application of magnetic actuation is limited by the requirement of external magnetic fields, which can be used for conventional microdevices and nanowire structures such as SiC nanowire, CNT nanotube and cantilever. 7) Optical gradient force is generated by a high-power laser beam, which produces a rapidly changing electromagnetic field. This field induces polarization or a dipole, leading to a force imbalance. This actuation method is commonly employed in the operation of optomechanical resonators.

Sensing or detection methods include: 1) Optical detection is based on the variation in the reflection intensity of an infrared laser beam directed onto the MMR structure. The laser focuses on the area of the MMR with the highest vibration amplitude, such as the red laser directed onto the free end of a resonant

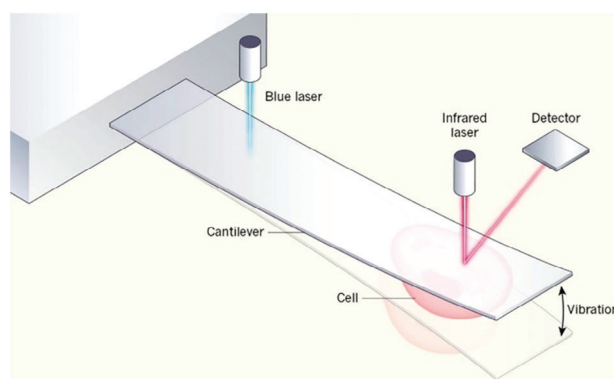


Figure 4. A representative example of optical actuation and sensing. Reproduced with permission. Copyright 2017, Springer Nature.^[51,52]

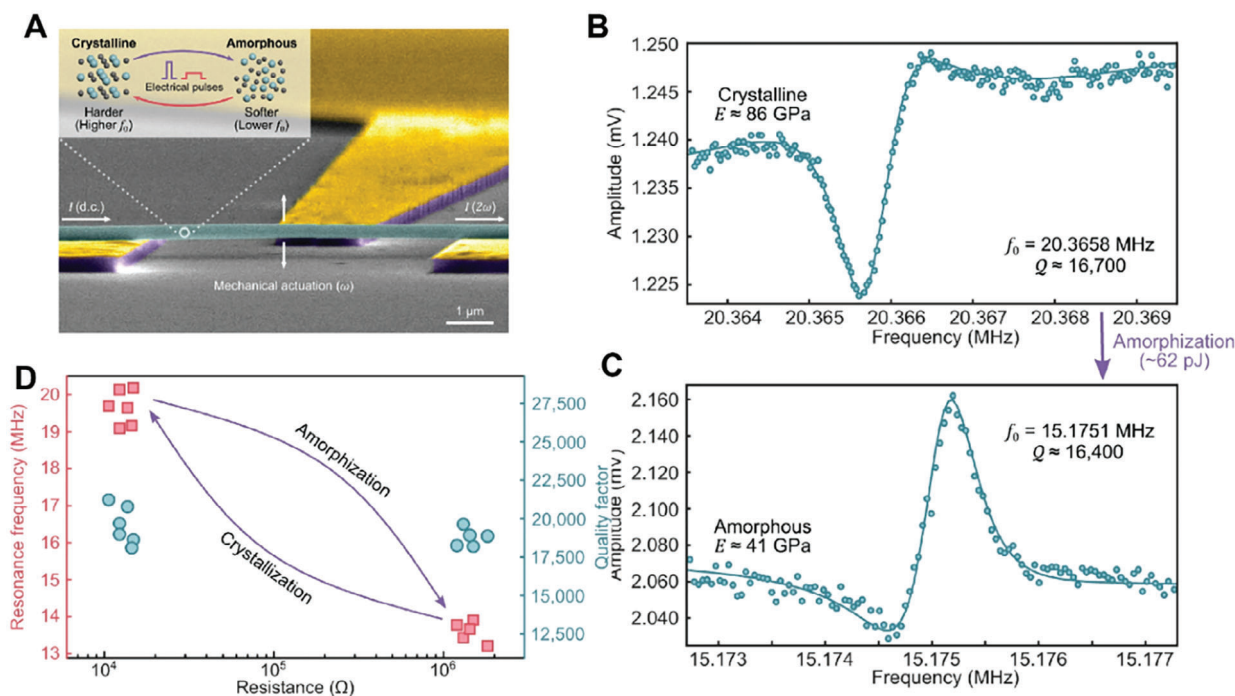


Figure 5. Impact of material morphology on resonance frequency and quality factor. Influence of material morphology such as crystalline and amorphous structures. A) A GeTe nanowire with a diameter of ≈ 300 nm is suspended and anchored by Au electrodes. Frequency response of B) crystalline and C) amorphous GeTe MMR nanowire. D) Cyclability test of the GeTe nanowires; the mean resonance frequency ratio between two phases is 1.45, and the Q is independent on crystallinity. Reproduced with permission. Copyright 2022, Springer Nature.^[17]

cantilever, **Figure 4**. Optical detection is very sensitive to device motion and offers a fast response. However, this method requires bulky and sophisticated laser systems and faces challenges in practical devices. 2) Piezoresistive detection is based on the change in resistance caused by induced stress and strain under vibration. This detection method requires the use of materials with good piezoresistive effect, typically found in semiconductors. To effectively utilize this method, the stress or strain must be induced on the piezoresistive element, which is located away from the neutral plane of out-of-plane resonant structures. In some cases, metals with a small piezoresistive effect, such as gold, are employed for nano MMR sensors. 3) Capacitive detection, also known as electrostatic actuation, relies on the change in capacitance between the MMR structure and a fixed electrode. This approach is widely used for both micro and macro devices. However, in nanodevices, a challenge arises due to the dominance of parasitic capacitance caused by the small relative size of the MMR structure compared to the fixed electrode. To address this challenge, a design incorporating frequency mixing devices has been employed. This design enables the mixing, modulation, amplification, and detection of the resonance information. 4) Inductive detection, which is the reverse of magnetic actuation, utilizes the change in magnetomotive voltage induced by the resonance in a magnetic field. 5) Piezoelectric detection involves detecting the motion of MMR sensors through the generation of voltage from a piezoelectric material under applied stress and strain.

In resonance sensors, the external physical inputs such as temperature, stress and mass will directly affect the mechanical prop-

erties of the MMR resonators, resulting in a change in measure outputs such as frequency, voltage or current.

2.3. Factors that Influence the Resonant Frequency and Quality Factor

To achieve a high figure of merit (FoM), it is necessary to have both high frequency and high quality factor. The following sections describe different factors that influence the quality factor and resonance frequency, as well as the recent advances made in relation to sensing performance.

2.3.1. Factors that Influence the Resonance Frequency

The resonance frequency primarily depends on intrinsic factors including the material morphologies, and the mechanical properties of the materials.^[53] Materials with higher Young's modulus and lower mass density, resulting in a higher acoustic velocity, exhibit a higher resonance frequency. Lowering mass density refers to reducing the mass of a material without changing its size or volume. Therefore, a material with a lower mass density will have a lower mass for a given volume, resulting in a higher resonant frequency. Therefore, various 1D and 2D materials such as carbon nanotube, nanowires, graphene, and MoS_2 , have been studied as excellent candidates for high frequency applications. For example, **Figure 5A** shows a suspended GeTe nanowire with a diameter of ≈ 300 nm anchored by Au electrodes. The resonance frequency of the nanowires depends on its morphologies,

with the crystalline phase having a higher resonance frequency (≈ 20 MHz) due to its higher density (6060 kg m^{-3}) and higher Young's modulus (86 GPa) compared to the amorphous phase, which exhibits a lower resonance frequency (≈ 15 MHz) resulting from its lower density (5600 kg m^{-3}) and lower Young's modulus (41 GPa), Figure 5B & C. The phase transformation does not result in any changes to the mass or length of the resonator.^[17] However, the transition between the amorphous and crystalline states causes a shift in the acoustic velocity of GeTe, leading to the observed change in the resonance frequency.^[17] Figure 5D summarizes the results of repeatability test of the GeTe nanowires, which shows the effect of material morphologies on the resonance frequency, quality factor and electrical resistance of the resonance structure. that the mean resonance frequency ratio between the two phases is 1.45.

The resonance frequency is also influenced by extrinsic factors, such as resonator geometry and external stress. To increase the resonance frequency, one approach is to miniaturize the MMR structure by designing it with a shorter length and larger cross-sectional area. Another method is to apply tensile stress to the MMR.

2.3.2. Factors that Influence the Quality Factor

A high-quality factor can be achieved by selecting materials with low levels of intrinsic dissipation. Crystalline materials, characterized by fewer defects, exhibit reduced internal friction and phonon-phonon losses.^[54,55] In contrast, amorphous materials, and those with high level of defects tend to have higher intrinsic dissipation and subsequent low-quality factor. However, in crystalline conductive materials such as metals and doped silicon, phonon-electron losses could significantly affect the Q factor. For example, GeTe conductive nanowires exhibited a negligible dependence of Q on material crystallinity (e.g., $Q = 16400$ for amorphous phase and $Q = 16700$ for crystalline phase, as shown in Figure 5).^[17] This suggests that although crystalline phase reduces the phonon-phonon losses, the increased phonon-electron losses prevent significant increase in the Q. In addition, intrinsic dissipations are temperature dependent. Operating at low or cryogenic temperatures reduces thermal noise and diminishes intrinsic losses. For example, resonators operating at low temperatures have been successfully employed for ultrasensitive force sensing applications.^[32,40,56]

Extrinsic dissipation arises from the interaction between MMR and the surrounding medium, including liquid and gases. This interaction impedes the motion of MMR as the energy is exchanged through molecular collisions. In the past, the dependence of Q on the density of the surrounding environment was utilized to measure the characteristics of the medium such as density and viscosity.^[57] To minimize energy loss, MMR resonators and sensors are conventionally operated under low-pressure or vacuum conditions to reduce the density of surrounding molecules. Under such conditions, carbon nanotube and other nanomechanical sensors have demonstrated unprecedented sensing resolution at the single-molecule level.^[58]

In addition to losses to the surrounding medium, vibration energy from MMR can dissipate into the substrate or supporting structures as a result of clamping or anchor forces. To mitigate

this, the MMR structure is usually suspended, with attachment to the substrate on a single side (e.g., cantilever) or two sides (e.g., doubly clamped beam). When MMR vibrates or resonates, it pulls on the clamping sides periodically, creating acoustic waves that carry the energy to the substrate, causing energy or leakage. The clamping losses can be reduced or even eliminated using an appropriate design of the resonance structures, clamping methods such as adhesive bonding or soft clamps, or allowing the MMR to rest under the fluence of gravity.

There is no doubt that achieving high performance sensing requires MMRs with high Q, which can be attained by minimizing both intrinsic and extrinsic losses. Popular approaches include manufacturing high quality crystalline materials, reducing temperature and pressure, and designing low-loss anchors. Recent advancements in strain engineering have achieved an ultrahigh quality factor of up to 10 billion in crystalline materials, which possess low internal friction, high intrinsic strain and high yield strength.^[59] Therefore, we anticipate the continuous effort to enhance Q by strain engineering of materials approaching their yield strength of materials, including SiC, graphene, and more. The combination of low mass (resulting in high resonance frequency) and high-Q MMR sensors presents a critical advancement toward quantum sensing and transduction. However, the need for cryogenic temperatures to minimize energy losses possess a challenge that must be addressed for practical applications.

2.4. Desired Characteristics of MMR Sensors

This section aims to provide a fundamental understanding of the desired characteristics that collectively contribute to the design of high-performance MMR sensors.

2.4.1. Resolution and Signal-to-Noise Ratio (SNR)

A high signal-to-noise ratio (SNR) is crucial for achieving a high sensing resolution as it represents a strong signal relative to the background thermal noise level, which is the primary source of noise in MMR sensors. The thermal displacement or "noise floor" is calculated as follows:^[60]

$$X_{th} = \sqrt{\frac{k_B T}{2\pi^3 m f^3 Q}} \quad (2)$$

where k_B is the Boltzmann constant; T is temperature; m and f are the mass and frequency, respectively. In MMR sensors, the SNR is determined as follows:^[60]

$$SNR = \alpha S \sqrt{\frac{Q}{4k_B T}} \quad (3)$$

where S , Q and α are the minimum of the signal, mechanical quality factor, and scaling factor, respectively. A higher Q leads to an increase in SNR, resulting in a higher resolution. In addition, a lower temperature contributes to improved SNR. For example, single carbon nanotube MMR force sensors achieved a high SNR of 17 dB at 300 mK, benefiting from low thermal fluctuation in cryogenic conditions.^[61]

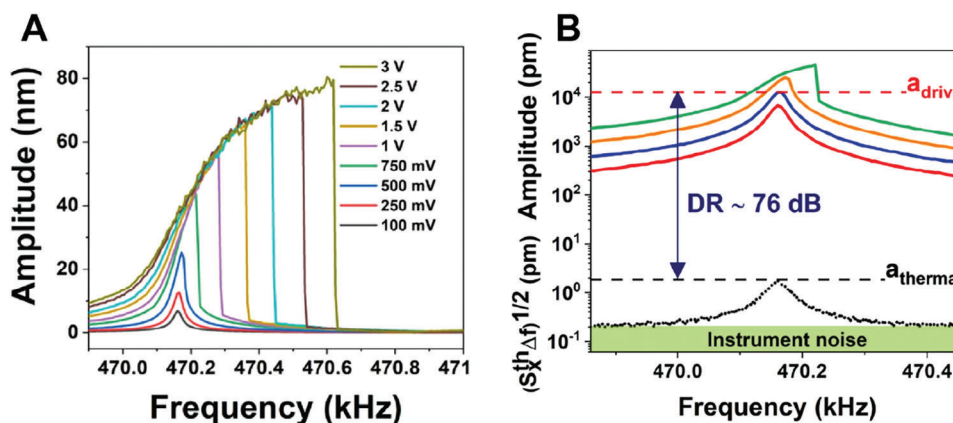


Figure 6. Frequency stability and dynamic range of a 3D printed NEM cantilever. A) Amplitude spectra of cantilever device, showing the dependence of resonance frequency on amplitude. B) Dynamic range between the amplitude of thermal noise spectrum and maximum linear driven signal. Reproduced with permission. Copyright 2021, Springer Nature.^[62]

2.4.2. Frequency Stability and Dynamic Range

Frequency stability is crucial for MMR sensors as it ensures stable and accurate measurements. Under certain conditions, the resonance frequency of an MMR remains independent of its amplitude when the driving amplitude is maintained within a certain range. However, geometrical nonlinearity (such as Duffing nonlinearity) can cause the resonance frequency to become amplitude-dependent when the driving amplitude exceeds a maximum level. For example, when a voltage exceeding 750 mV is applied to a piezo disk to drive a NEM cantilever into resonance (**Figure 6A**), the cantilever, which was 3D printed using neodymium-doped yttrium aluminium garnet (Nd:YAG), exhibits amplitude-dependent resonance frequency.^[62]

The frequency stability is predicted based on the following equation:

$$\frac{\delta f}{f_0} \sim \frac{1}{2Q} 10^{-DR/20} \quad (4)$$

where DR is the dynamic range estimated by the power difference between the maximum linear amplitude and the noise amplitude. It is expected that an increase in both mechanical quality factor Q and dynamic range DR will correspondingly enhance the frequency stability. **Figure 6B** shows an example of a dynamic range of 76 dB which was determined by comparing the power levels of signals originating from thermal and driving vibrations. A broad DR allows the resonator to effectively respond to a wide range of input signals. Scaling down 1D NEMS structures typically results in a lower DR or limited DR.^[63] Thanks to the atomic layer structure, 2D materials such as molybdenum disulfide (MoS_2) achieved a DR as high as 110 dB.^[64]

2.4.3. Bandwidth

Bandwidth refers to the frequency range within which the MMR sensor can effectively transduce the signals. For accurate measurement of changing signals, a wide bandwidth is required. However, there is a trade-off between achieving a high SNR and

a wide bandwidth. To increase the bandwidth while maintaining the SNR, it is common to suppress the quality factor. If a feedback force $f_{fb} = -b' \dot{x}$ is applied to the resonator, where b' is an effective damping constant, the quality factor is modified and known as an effective quality factor $Q_{eff} = \sqrt{km} / (b + b')$. By introducing a positive b' , $Q_{eff} < Q$, the quality factor is suppressed; if b' is negative, $Q_{eff} > Q$, the quality factor is enhanced. It is noted that increasing the mechanical Q leads to an increase in SNR and decrease in thermal noise X_{th} . However, an increase in Q_{eff} only modifies the noise spectrum near resonance. More details on effective quality factor tuning mechanism can be found in the review paper.^[60]

2.5. Frequency Tuning in MMR Sensors

The resonance frequency is a key parameter to evaluate performance of resonant devices and is desirable to have a large tuning range for sensing and other MEMS/NEMS applications. Achieving a large tuning range requires attention to various factors, including mechanical material properties and residual stresses. Tunability of resonance frequency has attracted considerable interest for sensing applications, with MMR sensors and resonators based on 2D nanomaterials demonstrating a resonance tuning range $\Delta f/f_0$ of above 200% through the application of tensile stress to the structures.^[65] The tuning range reached 230% (from 2.78 to 9.21 MHz) using a gate voltage to induce a tensile stress to the 2D NEMS structure.^[65] High tuning sensitivity of 1–100 GHz ϵ^{-1} was also achieved.^[66,67] **Figure 7A** shows an example of the frequency tunability of ultrathin resonant beams, where the fundamental frequency depends on the length of the nanobeam (inset) and the residual stress of the resonating stack resulting from patterning and then transferring of the beam. The thermomechanical responses are dependent on stress induced by irradiation, **Figure 7B**. Ultra-wide frequency tuning range can be achieved for thin nanomechanical resonators by tuning the aspect ratios of length/thickness (L/t) and applying strain to the structure.^[68] With a well-designed resonant structure and applied stress, the resonant frequency can be precisely controlled within a wide tuning range, **Figure 7C**. Resonant

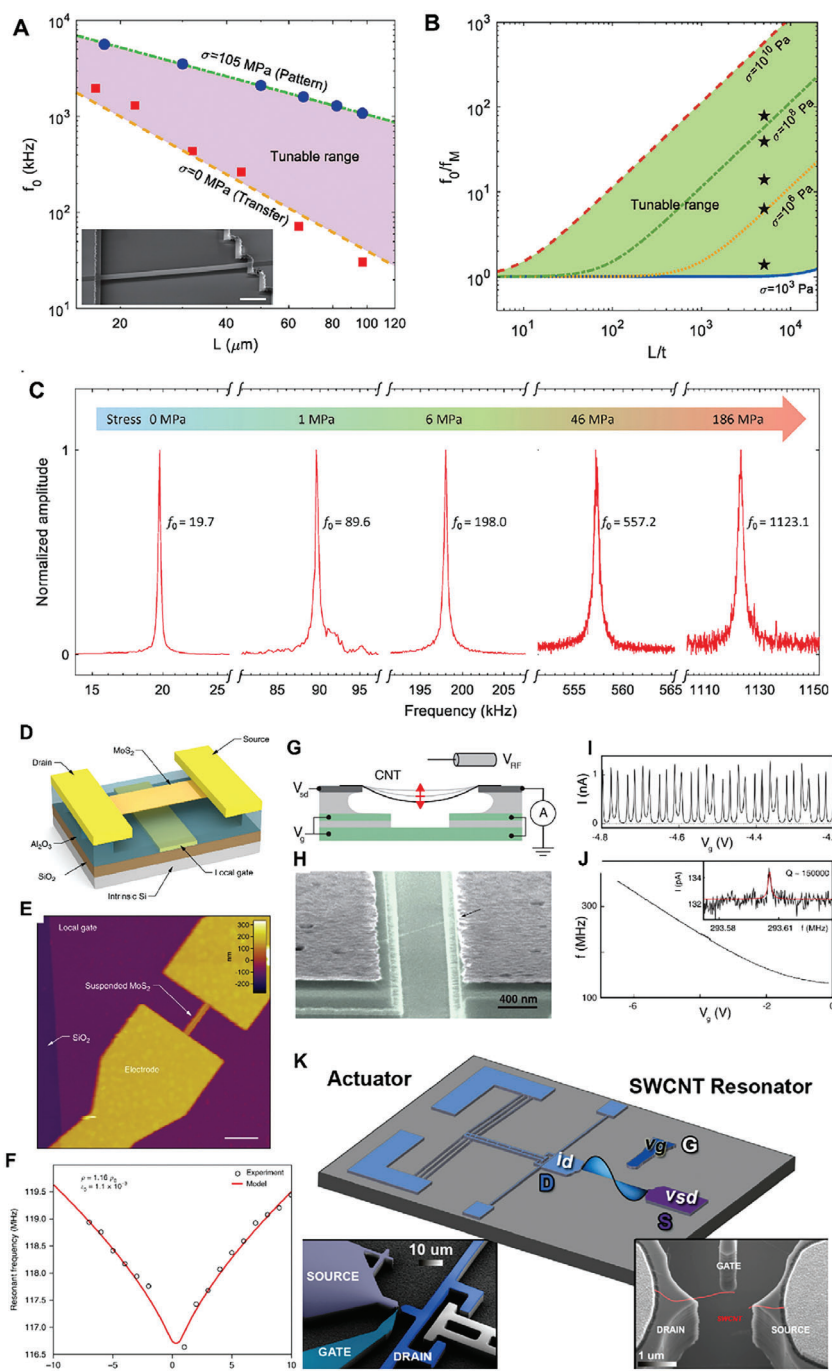


Figure 7. Frequency tuning of nanoscale resonant sensors. Frequency tunability of ultrathin resonant beams with A) fundamental frequency dependence on the length of beam L , stress (patterned and then transferred, inset shows the nanobeam) and B) thermomechanical responses which are dependent on stress induced by irradiation. C) Dependence of frequency on stress. Adapted with permission.^[68] Copyright 2020, American Chemical Society. D) Schematic of monolayer MoS_2 resonant structure with a local gate to introduce electrostatic forces. E) AFM image of a monolayer MoS_2 ribbon suspended. F) Change of the resonant frequency under tensile strain $\epsilon_0 = 1.1 \times 10^{-3}$. Adapted with permission.^[72] Copyright 2019, Springer Nature. G) Electrostatic actuation of a single CNT using a gate voltage. H) A single CNT suspended on Pt electrodes. I) Coulomb current measured from CNT under bending-mode resonance. J) Tuning frequency of a single CNT by gate voltage. Adapted with permission.^[76] Copyright 2009, American Association for the Advancement of Science. K) External stress and strain are induced on CNT by a V-shape electrothermal actuator. Adapted with permission. Copyright 2014, American Chemical Society.^[66]

frequency tuning can also be achieved through a combination of the residual stress resulting from growth of nanofilms and the Joule heating effect.^[69] For example, the residual stress between SiC nanofilm and Si substrate can cause buckling in the out-of-plane direction,^[70] with increasing thickness reducing the impact of buckling. Residual stress in SiC/Si nano thin films has been demonstrated to increase the resonant frequency and quality factor.^[71]

Recent research has made significant progress in utilizing 2D materials for MMR sensors, enabling ultra-high frequency tunability through the application of stress or strain. These highly-tunable 2D MMRs are often designed in the form of membranes. For example, a MoS₂ stress sensor controls tension by using a DC gate voltage to deflect the membrane, as shown in Figure 7D,E.^[72] Remote actuation with on-chip capacitors is recently shown as potential method to actuate the membrane structure.^[73] Figure 7F demonstrates the measured resonance frequency of MoS₂ as a function of the gate voltage, with an estimated built-in strain of $\approx 10^{-3}$.^[72] Joule heating has been utilized to tune the frequency of MoS₂ up to 123%V⁻¹.^[74] Fringing electrostatic fields have been also used to control the bi-stability and tune the enhance the frequency sensitivity.^[75] Graphene and other 2D materials have also been demonstrated as sensitive mass sensors, offering high Q value of 14 000, a resolution of 2 zg, and a large area of detection for capturing mass flux.^[68] These advancements are significant steps toward the development of highly sensitive resonant force and strain sensing. However, to realize the practical application of MMR structures with high frequency and tuning range, chip-level integration of devices is required to enable their coupling with external measurands and applied strain/forces.

The frequency tuning in 1D structures (nanowires and nanotubes) can be achieved by controlling external forces or stresses.^[77,78] By applying a gate voltage, similar to other atomically thin resonators, the frequency of the nanostructure can be tuned.^[72,79] Figure 7G,H. In carbon nanotubes (CNTs), Schottky barriers created by Pt metal electrodes confine electrons, leading to a peak in the measured current at resonance when a periodic radio frequency potential is applied using an antenna,^[76] Figure 7I. By applying a gate voltage, a tuning ratio of 2x for the resonance frequency of a single CNT was achieved, Figure 7J. Carbon nanotube mechanical resonators have demonstrated ultra-high frequencies of 4.2–39 GHz by introducing tensile stress in the nanotube.^[1,80] Various methods, such as suspending CNTs between AFM tips or supporting substrates, or using an integrated V-shape electrothermal actuator, allow for the introduction of tension or compression to control the stiffness of the MMR structure.^[67,81] The tensile stress can be controlled by an integrated V-shape electrothermal actuator that pulls the CNT and changes its stiffness, Figure 7K.^[66] This technique enables a large tuning frequency range of above 200%.^[66,67]

3. Scaling of MMR Sensors: Advanced Nanomaterials and Fabrication Techniques

The recent research on MMR sensors has focused on three main areas: miniaturization of structures, utilization of new materials, and the development of advanced designs and structures. In this section, we explore the impact of scaling down the dimensions of MMR sensors and the influence of nanoscale materials and

structures on their mechanical properties and performance. Additionally, we discuss various fabrication techniques employed to create these miniaturized MMR structures, as well as recent advancements in alternative fabrication methods like 3D printing.

3.1. Effect of Scaling Down the Dimensions on the Property of MMR Sensors

Scaling down MMR sensors to nanometric dimensions reduces their mass *m*, resulting in ultra-low mass devices and an increase in the resonance frequency. This low mass allows the sensor to exhibit a large change in the resonance frequency in response to small perturbations. Nanomechanical sensors have been successfully operated in a Giga Hertz (GHz) range, enabling ultra-fast response to the measured quantities. In the case of cantilever-type resonators, reducing the length of the MMR by an order of magnitude increases the resonance frequency by two orders of magnitude. Specifically, the frequency of a cantilever is directly proportional to its thickness (*t*) and inversely proportional to the square of its length *L* as: $f \sim t/L^2$. The miniaturization capability of MMR sensors enables high-resolution detection of mass and force. When the sensor dimensions are scaled down, the mass resolution improves according to the equation $\Delta f = (\Delta m/2m)f$. As a result of scaling down, the resonance frequency increases and the effective mass decreases. Therefore, nanoscale MMR sensors offer high-frequency operation, unprecedentedly fast response, and ultra-high resolution/sensitivity.

By shrinking the dimensions of MMR sensors to the nanometer range, the surface area increases relative to the volume, resulting in a higher surface-to-volume ratio. The surface properties become crucial in this context. At the nanoscale, such as with a thickness of 100 nm or below, MMRs exhibit significant surface stress, strain, and energy due to the absence of bonding between surface atoms and the environment. As a result, the surface properties of MMRs play a vital role in their mechanical and electrical characteristics, including the resonance frequency. One key impact of surface properties on MMR sensing is the absorption of molecules onto the surface, which can alter bonding and surface stress. Extensive efforts have been made to understand the effect of surface stress or energy on the resonance frequency of MMRs, but the results are still controversial. Theoretical studies suggest that surface stress significantly influences the resonance frequency and sensitivity of nanoscale MMR sensors.^[82,83] However, experimental research has shown that the resonance frequency of nanoscale cantilevers is independent of surface stress,^[84] while doubly clamped nanobeams exhibit a strong dependence on compressive stress.^[85] The discrepancy between the theoretical and experimental observations can be attributed to the absence of a successful direct measurement of relationship between surface stress and resonant frequency.^[84] This is compounded by the fact that the surface stress is the result of a combination of axial and bending stresses as well as their coupling, which is challenging to incorporate into these theoretical models.^[86] While it is expected that doubly clamped beams are more sensitive to surface stress than cantilever beams, accurately understanding the role of surface stress in the motion of any MMR will improve the accuracy of data interpretation for biological and chemical species.^[86]

Advancements and challenges: One example of an extremely small MMR sensor is a single carbon nanotube (CNT) with a radius of 1.5 nm and a length of 150 nm. This nanotube operates at a resonance frequency of 2 GHz and demonstrates the capability to effectively probe the mass of a single proton, which is ≈ 1.7 yg ($1 \text{ yg} = 10^{-24} \text{ g}$).^[87] Ultrasensitive resonant sensors have demonstrated successful measurements of temperature, infrared wavelength, and inertial forces. MMR sensors based on 1D and 2D materials show promise in terms of small device footprint and ultrahigh sensitivity, thanks to their low mass. However, the sensitivity of nanomechanical sensors also makes them susceptible to perturbations. To ensure accurate measurements, these sensors often require cryogenic and low-pressure conditions, posing challenges for practical applications that necessitate room-temperature operation. Operating MMR sensors at room or elevated temperatures can lead to degradation due to higher levels of thermal noise.

The role of the surface in the motion characteristics of MMR sensors still requires attention. First, it is important to address how to control the surface quality and uniformity during fabrication. Second, systematic studies are needed to understand the impact of surface bonding and defects on the performance of MMR sensors. It is anticipated that improving surface quality will reduce internal losses and interaction losses between the MMR structure and its environment or samples, leading to enhanced readout signals and measurement reliability at the nanoscale.

3.2. The Role of Nanomaterials and Nanostructures

MMR sensors make use of semiconductors, carbon nanomaterials, and 2D materials. Advancements in nanotechnology have allowed MMR sizes to be scaled down to the nanometer and atomic levels, in the form of 1D structures (nanotubes and nanowires) and 2D structures (such as graphene and other 2D materials).^[88,89] These materials are chosen for MMR sensors due to their large elastic modulus, which is crucial for achieving high resonance frequencies. With high Q factors and low mass, these MMR sensors offer exceptional sensitivity. Consequently, nanoscale MMRs provide a powerful tool for probing the mechanical, electrical, optical, and magnetic properties of new materials like titanium carbide (MXene), transition-metal dichalcogenides, and graphene.^[90,91]

Ultra-thin MMRs based on 2D materials have extremely low mass, allowing for significant changes in resonance frequency in response to added mass. Recent investigations have demonstrated the detection capability of a single layer of MXene with a thickness of 0.98 nm and an effective modulus of 5.9 TPa. This MXene-based MMR sensor exploits its piezoelectric properties to precisely measure the weight of ultra-small molecules, achieving a mass resolution of 0.2 Zeptograms.^[90] Graphene, with a monolayer thickness of 0.335 nm and a Young's modulus of ≈ 1 TPa, has been demonstrated for MMR mass and temperature sensing.^[39] Monolayer and few-layer MoS₂ with excellent mechanical properties (nanometer-scale thickness and elastic modulus of 0.2–0.3 TPa) have been studied to understand strain- and dynamics-engineered ultra-thin semiconducting 2D crystals.^[72,92] At the sub-nanometer scale, the resonance motion of MMRs is influenced by built-in strain induced by the substrate

and supporting structures (electrodes). Monitoring the motion of nanoscale MMRs offers insights into mechanical interaction effects, paving the way for the development of ultra-sensitive force and mass sensors.^[72]

Semiconductor nanowires^[93,94] and nanocantilevers^[95] and carbon nanotubes have been widely used as core resonant structures in MMR sensors. These structures possess ultra-small sizes, ranging from a few nanometers to a few hundred nanometers, resulting in a large surface-to-volume ratio. In many cases, the miniaturized nanoscale structure exhibits a small effective mass comparable to the mass resolution of MMR sensors^[38,96] For instance, a carbon nanotube with a radius of 1.5 nm and a length of 1 μm has an effective mass in the zeptogram range (≈ 7 zg),^[38] which is equivalent to ≈ 30 xenon atoms or the mass of an individual 4 kDa molecule. Doubly clamped SiC nanowires also demonstrate a similar mass resolution.^[96] Due to their high conductivity, semiconductor nanowires and carbon nanotubes allow electrical currents to pass through them, providing opportunities for utilizing electrical signals for excitation and detection rather than relying on optical methods. A wide range of nanowires and nanobridges made from various MEMS/NEMS materials, including Si,^[93,97–99] SiC^[100,101] and GaN,^[102–104] have been employed as sensing element in MMR sensors.

Advancements and challenges: The unique feature of scaling down MMR structures is the ability to create low-mass structures, which offers greater opportunities for tuning the resonance frequency and achieving higher sensitivity. As a result, 1D and 2D materials have garnered significant interest for sensing applications due to their small thickness or low effective mass. Various 1D structures such as nanotubes and nanowires have been successfully fabricated and demonstrated for sensing with state-of-the-art performance. Recently, 2D materials like graphene, MoS₂, and MXene have also been explored for sensing applications, with the potential for discovering new materials. By utilizing high Young's modulus materials, MMR sensors can operate at ultrahigh resonance frequencies. However, scaling down the size of MMR sensors presents challenges, including:

Low Q-factor due to internal losses such as thermomechanical effects and external losses including damping. Consequently, nanoscale MMR sensors with high Q-factors are typically designed for low-temperature conditions (cryogenic temperatures).

The small size of MMR sensors makes the detection of their motion more challenging. Optical measurement of nan surface stress on wires and nanotubes is difficult because the laser spot size is typically larger than the width of the resonant structure, resulting in low reflected light density and weak signals compared to background noise. In contrast, electrical detection by applying an electrical signal along the axis of the nanowire/tube is preferred.^[100] Optical measurement is suitable for 2D materials.

3.3. Fabrication of MMRs

3.3.1. Standard Top-down MEMS/NEMS Fabrication

Standard top-down techniques are commonly used to create micro and nanostructures by selectively removing materials. This process involves applying a mask to a functional layer supported by a substrate. Conventional lithography processes,

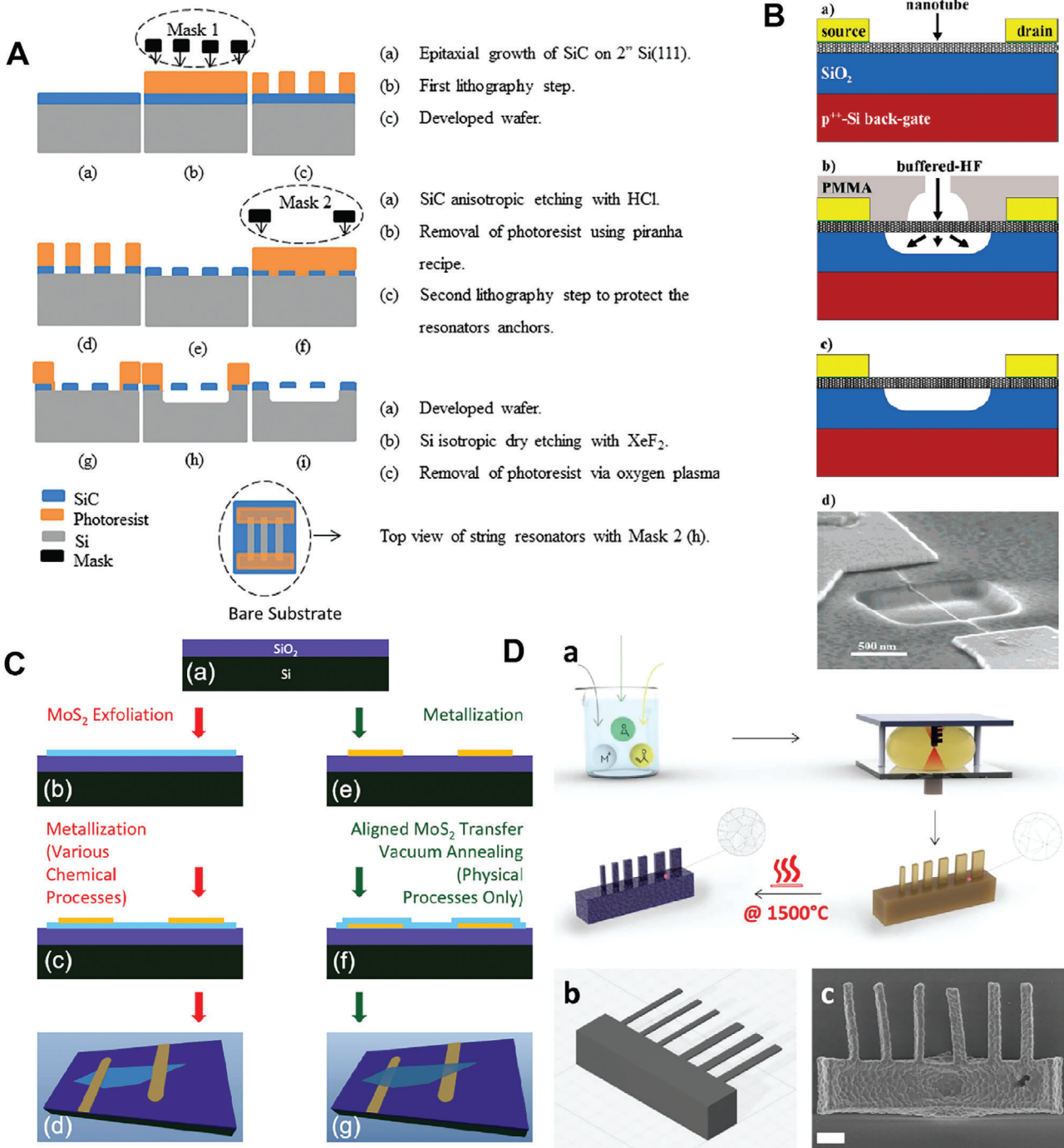


Figure 8. Fabrication of MMR sensors. A) A representative conventional top-down fabrication of micro and nanostructures. Adapted with permission.^[71] Copyright 2014, American Institute of Physics. B) A hybrid bottom-up (CVD) growth of CNT and top-down patterning of electrodes for single CNT MMR sensor. Adapted with permission.^[112] Copyright 2006, American Chemical Society. C) Fabrication of MMR based on 2D flakes. Adapted with permission.^[113] Copyright 2014, American Institute of Physics. D) 3D printing of nanostructures. Adapted with permission. Copyright 2021, Springer Nature.^[62]

including aligner lithography,^[105] laser-direct write,^[106] and step-lithography,^[107] are widely employed for fabricating resonant structures with larger sizes ranging from a few micrometers to hundreds of micrometers. Advanced nano lithography techniques such as electron beam lithography (EBL) offers high-

precision patterning down to the nanoscale.^[69,108,109] For example, **Figure 8A** illustrates a representative fabrication process of SiC resonators, starting with the growth of SiC nanofilm, patterning of photoresist, followed by etching of SiC. The second lithography process is utilized to protect anchors and support to

release the SiC structure from the substrate by dry etching of the Si substrate. In addition, focus ion beam (FIB), which employs a high-energy beam of ions to remove materials, is a powerful tool for patterning micro and nanostructures of ceramic and hard materials.^[110] Nanomechanical sensors have been fabricated using FIB to etch down large structures. However, surface damage caused by FIB may limit the quality factor and subsequent performance of nanomechanical sensors.^[111] Therefore, to enhance the detection accuracy of top-down fabricated MMR sensors, nanofabrication techniques with high precision are required.

3.3.2. Standard Bottom-Up and Hybrid Fabrication

Bottom-up methods involve the growth of nanostructures on a substrate using a precursor. For nanomaterial-based MMR such as CNTs, the material is first grown through vapor–liquid–solid (VLS)^[114] or chemical vapor deposition techniques (CVD).^[112] Subsequently, the single-wall CNT position on the substrate can be located using atomic force microscopy (AFM), and metal electrodes are deposited via electron beam lithography (EBL). This is followed by an etching process to suspend the CNT. An illustration of this process is shown in Figure 8B. Alternatively, the transfer of CNTs can be achieved using stamping methods.^[115] Finally, the CNT is suspended by wet etching of SiO₂. This process combines both bottom-up (CNT growth) and top-down (EBL and etching) methods. A similar hybrid approach is employed for fabricating MMR resonators using 2D materials. Figure 8C illustrates the representative process for fabricating MoS₂ MMR resonators. The 2D flakes are typically exfoliated and positioned on a substrate before the top-down method is employed to pattern electrodes on the structure. Unlike top-down fabrication, which can cause surface damage and degrade the performance of nanomechanical sensors, bottom-up methods can produce high-quality nanostructures with a high quality factor and resonance frequency in the several hundred megahertz range.^[116]

3.3.3. Other Fabrication Techniques

Conventional MEMS/NEMS technologies often involve complex and expensive nanofabrication processes, which limit the widespread application of MMR sensors. As an alternative, various fabrication technologies have been proposed, including additive manufacturing (e.g., 3D printing) and conventional printing, which offer advantages such as easy fabrication, rapid prototyping, low cost, and accessibility. For instance, gravimetric sensing utilizing resonant microcantilevers with different geometries ($1 \times 1 \times 0.1 \text{ mm}^3$ to $8 \times 2 \times 0.1 \text{ mm}^3$) has been achieved through screen-printing techniques, enabling a low limit of detection of 70 ng at a resonant frequency of 680 kHz.^[117] MMR sensors have also been fabricated using methods like hot embossing, microinjection molding, solvent casting, nanoimprinting, microfluidics, and 3D printing.^[62] These fabrication methods are well-suited for polymeric materials characterized by a low modulus of elasticity and suboptimal material quality, resulting in resonator devices fabricated by these methods exhibiting a high loss factor, consequently leading to significant reduction in the quality

factor. Therefore, most of these studies have shown lower sensing performance compared to traditional MEMS/NEMS resonant sensors.^[62] Due to low fabrication precision, these methods have also faced challenges in fabricating miniaturized structures, restricting their size to the micrometer range. This limitation leads to a large mass and subsequently, low resonant frequency. Recent research has demonstrated that two-photon printing lithography (TPP) can be employed to fabricate nanoscale MMR sensors with high-frequency operation and high-quality factor. This approach involves selectively polymerizing a precursor solution ink using an ultrafast laser. Figure 8D illustrates the rapid printing of nanoscale MMR sensors using TPP.^[62] After polymerization, the material is transformed into a rigid crystalline structure through heating at 1500 °C. The 3D-printed MMR mass sensor exhibited a mass sensitivity of 450 zg, which is comparable to the performance of silicon-based NEMS sensors.^[62]

3.3.4. Advancements and Challenges

To date, various fabrication strategies have been employed to scale down the size of MMR sensors. Conventional top-down and bottom-up approaches involve processes such as lithography, etching, transferring, and releasing to create suspended resonant structures. However, scaling down MMR structures presents several challenges, including:

Fabrication and manipulation of materials and structures at the nanoscale are inherently challenging. While conventional materials like Si and some semiconductors have well-established fabrication processes comparable to MEMS/NEMS, many MMR sensors require growing materials on one substrate and then transferring the resonant structures to another platform for interconnection. Inconsistencies in device fabrication and performance hinder research and development of these MMR sensors on a small-scale production. Practical applications necessitate large-scale growth approaches capable of producing high-quality materials at the wafer level. For thin films and 2D materials, it is crucial to achieve high-quality single-crystalline and uniform materials for consistent device performance. For instance, SiC nanofilms can be grown on Si substrates with high-quality crystalline structure and uniform thickness. However, challenges arise from defects at interfaces and lattice mismatches between SiC and Si, which impact the uniformity of device performance.^[71]

Scaling down MMR structures necessitates further advancements in miniaturization capabilities and poses significant challenges in nanofabrication to achieve nanometric and atomic scales in all three dimensions (thickness, length, and width). We anticipate various technical challenges in fabricating such small structures with high resolution, as well as challenges in handling, measuring, and achieving large-scale manufacturing.

The fabrication challenges also extend to other techniques, including 3D printing in the nanometric range. Improving the crystalline material quality of 3D-printed MMR sensors is essential to enhance the quality factors and resonant frequencies. There is a strong interest in developing 3D printing techniques for MMR sensors to cater to diverse applications.

Recent advancements in Artificial Intelligent (AI) have enabled efficient fabrication of MMR sensors such as CNT based

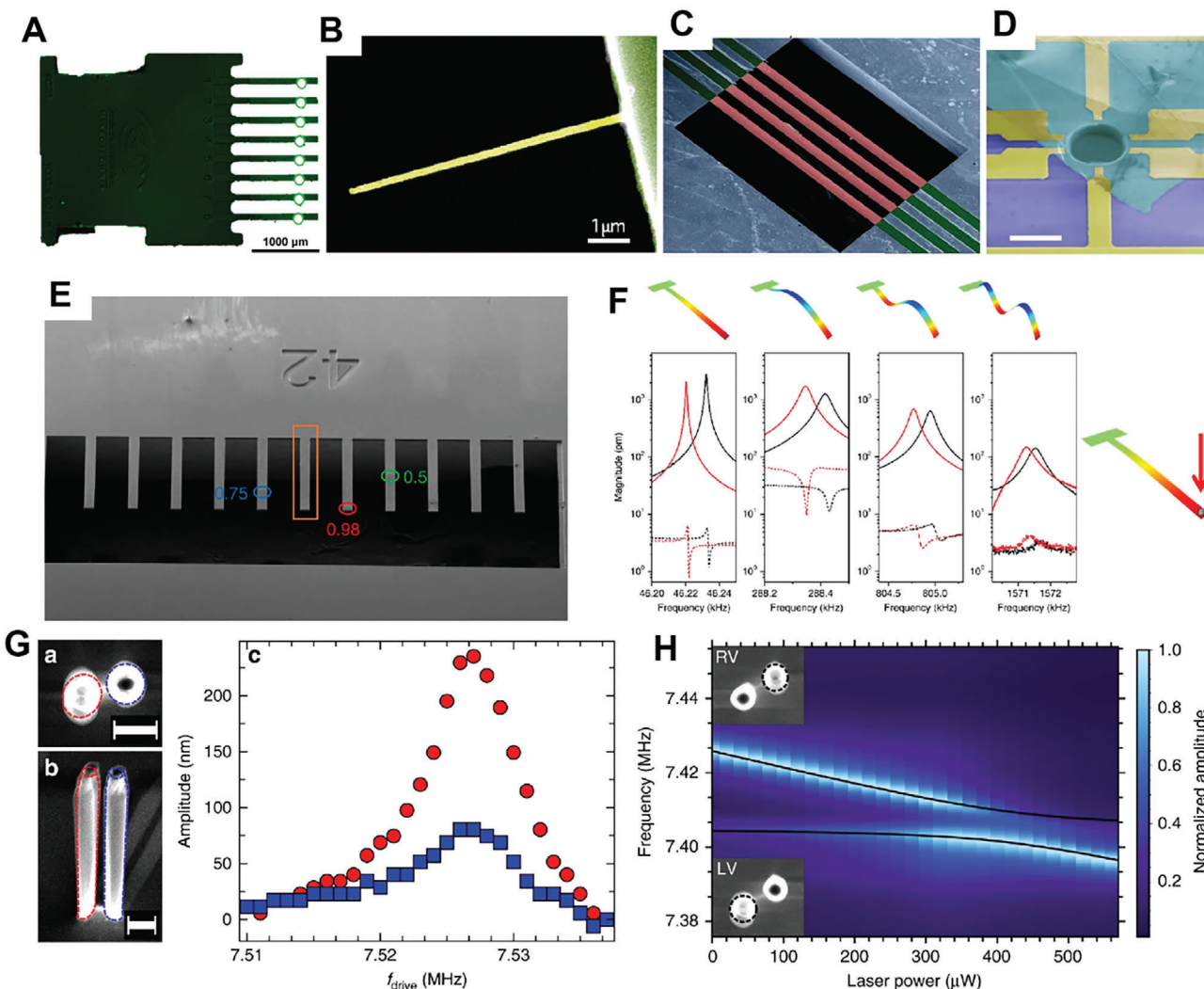


Figure 9. Conventional design of MMR structures. A) Design of cantilever array. Adapted with permission.^[119] Copyright 2022, Elsevier. B) Silicon nanowire cantilever for mass sensing. Adapted with permission.^[41] Copyright 2010, Springer Nature. C) Doubly clamped beam silicon carbide array. Adapted with permission.^[69] Copyright 2022, Elsevier. D) Circularly clamped h-BN MMR. Scale bar 10 μm . Adapted with permission.^[120] Copyright 2017, Springer Nature. E) Design of cantilever array for weak coupling in cantilever array and F) comparison of the resonance peaks and coupling peaks when a mass is added to the free end. Adapted with permission.^[25] Copyright 2019, Springer Nature. G) Design of two pillars for strong coupling: SEM of pair of nanopillars (left) at top and 60° tilted views, and amplitude for different drive frequencies. H) Frequency response measurements showed strong coupling. Adapted with permission. Copyright 2019, Springer Nature.^[121]

nanocantilever.^[118] Deep neural network can be utilized to recognize single CNTs and automatically and accurately determine their positions (accuracy >90%). AI is expected to contribute to more efficient fabrication methods for large scale and complex devices.

4. Design of MMR Structures

Recent research has focused on optimizing structures and geometries to minimize energy losses and implement dissipation dilution. This section presents the latest design strategies, including soft clamping and strain engineering, which enable the development of ultra-high Q MMR sensors.

4.1. Conventional Structure Designs

The popular MMR structures include cantilever and its array (single-clamped),^[119] bridges (doubly clamped),^[69] and circularly clamped membrane.^[122] Cantilever-based MMR sensors feature a free end that can accommodate a tiny tip, enabling high-performance force sensing and continuous monitoring of surface forces during mass and chemical species measurements. Their small size also makes them suitable for fast and label-free biosensing. Cantilever arrays (Figure 9A) offer diagnostic screening and analyte monitoring capabilities, as well as the ability to probe analytes absorbed at greater distances from the sensing cantilever.^[25] For higher sensitivity and resolution, cantilevers can be scaled down to the nanometric range (Figure 9B). CNT cantilevers, for instance, are among the smallest MMR structures

demonstrated for mass sensing, achieving a resolution up to zeptograms,^[58] surpassing the performance of silicon nanowire cantilevers.^[41]

Doubly clamped beams offer higher resonant frequencies compared to cantilever configurations. Strategies such as dissipation dilution and strain engineering can be employed to enhance the resonant frequency and quality factor of these bridges.^[53] Figure 9C showcases doubly clamped SiC bridges that demonstrate a significant tuning range of up to 80% in resonant frequency.^[69] Doubly clamped MMR structures based on carbon nanotubes (CNTs) exhibit high working frequencies reaching up to 100 MHz.^[112] The design of bulked CNTs can yield lower resonant frequencies while offering bi-stability and spectral broadening for sensing and other applications.^[22] Conventional circularly clamped membranes, on the other hand, possess the advantage of high resonant frequencies.^[122] This configuration is commonly utilized in 2D materials with naturally occurring nanoflake structures, enabling easy actuation using electrostatic forces,^[120] Figure 9D. Recently, squared membrane resonators have been demonstrated for high-throughput mass sensing at single cell level.^[123] Moreover, coupling 2D nanomaterials with circular cavities allows for tuning the properties of the MMR structure.^[124]

The mechanical coupling of MMR sensors has garnered significant interest in sensing applications. In the case of a cantilever array (Figure 9E), a weak coupling allows the sensing cantilever to be positioned at a distance from the cantilever that absorbs mass,^[121] Figure 9F. Alternatively, a pair of micropillars can offer strong mechanical coupling, facilitated by the joint substrate,^[121] Figure 9G & H.

Advancements and Challenges: To date, various strategies have been employed to support resonant structures, including single-clamp, double-clamp, and circular-clamp configurations. Single-clamped structures, such as cantilevers, are widely used for force and biological sensing. The cantilever tip is well-known in atomic force microscopy for its high-frequency operation and exceptional sensitivity. The free end of the cantilever can be designed to accommodate biomolecules, enabling label-free detection in bio applications. Double-clamped structures, like bridges, allow for the introduction of large tension to tune the resonance frequency. Various methods, such as electrothermal and electrostatic forces, can induce strain or deflection, resulting in frequency changes. Circular-clamped structures are typically used for 2D materials, including graphene and MoS₂, as their resonance frequency can be easily controlled by a gate voltage. Recent research focuses on fabricating arrays of these structures to enable mechanical coupling of their motion. The degree of mechanical coupling determines the novel features that MMR sensors can offer for traditional sensing applications. Designing and fabricating uniform arrays of nanostructures and devices, especially at large scales, pose challenges. Achieving coupling or decoupling of mechanical motion in large arrays will be crucial for chip-level applications and practical implementation.

4.2. Rational Design of MMR Structures

Recent research has driven toward optimization of structures and geometries to reduce energy losses or implement dissipation di-

lution. This section presents the most recent design strategies such as soft clamping and strain engineering that enable ultra-high Q MMR sensors (up to 10 billion so far).

4.2.1. Design of Soft Clamp Geometry

The principle of dissipation dilution through soft clamping aims to reduce energy losses caused by bending in MMR sensors during operation. One example is the design of Si₃N₄ nanobeams, as shown in Figure 10A, where tapering the clamping points increases the Q factor by a factor of 2.4.^[125] The Q factor decreases with larger clamp radii for perpendicularly oriented strings, while a slight increase is observed with smaller radii in diagonally oriented strings.^[128] These soft clamping methods demonstrate Q factor improvements of up to three times, resulting in large Q factors in the range of a few million. More recently, the use of hierarchical structures has pushed the Q factor to over 100 million and achieved a Qxf product above 10¹³ Hz, as depicted in Figure 10B.^[20] These hierarchical structures are designed using computer-aided topology optimization, enabling the optimization of MMR sensor geometry for maximum performance, as shown in Figure 10C. Moreover, Bereyhi et al.^[127] implemented a structural hierarchy design to achieve an unconventional form of soft clamping in resonance structures. Figure 10D showcases binary tree beams with varying branching numbers, resulting in a record-breaking Q factor of 7.8 × 10⁸ and force sensitivities of 740 zN/Hz^{1/2} at room temperature and 90 zN/Hz^{1/2} at 6 K. Together experimental works, numerical topology optimization^[129,130] and the thermodynamic design methodology^[131] has been proposed to optimize the f_xQ of substructural micro/nanoresonators, reaching 10¹³ Hz.^[130]

4.2.2. Rational Design for Strain Engineering

The strain engineering method aims to reduce energy losses by introducing more tensile energy into the resonance structure. When an MMR vibrates in the out-of-plane mode, the direction of tensile stress is perpendicular to the motion, resulting in no work done by tension and no energy losses. In recent years, designs of hierarchical structures for strain engineering have been proposed to implement tensile stress on the core MMR structure. Strain engineering involves a design approach that allows for high stress concentration on the MMR structure, up to the yield strength of the material. Traditionally, stress concentration in a specific area can be achieved by reducing the cross-sectional area, such as narrowing the width as seen in the dogbone structure shown in Figure 11A.^[132] The stress amplification factor between the nanowire σ_n and its substrate σ_{sub} is $K = \sigma_n / \sigma_{sub} = 1 / (1 - \frac{w_n - w_n}{w_n} \frac{L_m}{L})$, where w_m , w_n , L_m and L are the width of microframe, width of nanowire, length of microframe and total length, respectively.^[132] his relationship demonstrates a stress concentration factor of 6.^[132]

The strain engineering was successfully implemented in MMR through growth process of different materials such as SiC and Si₃N₄. Ensil stress, typically residual stress between thin film and substrate, is induced by the thermal mismatch between the MMR materials and the substrate when they are grown at

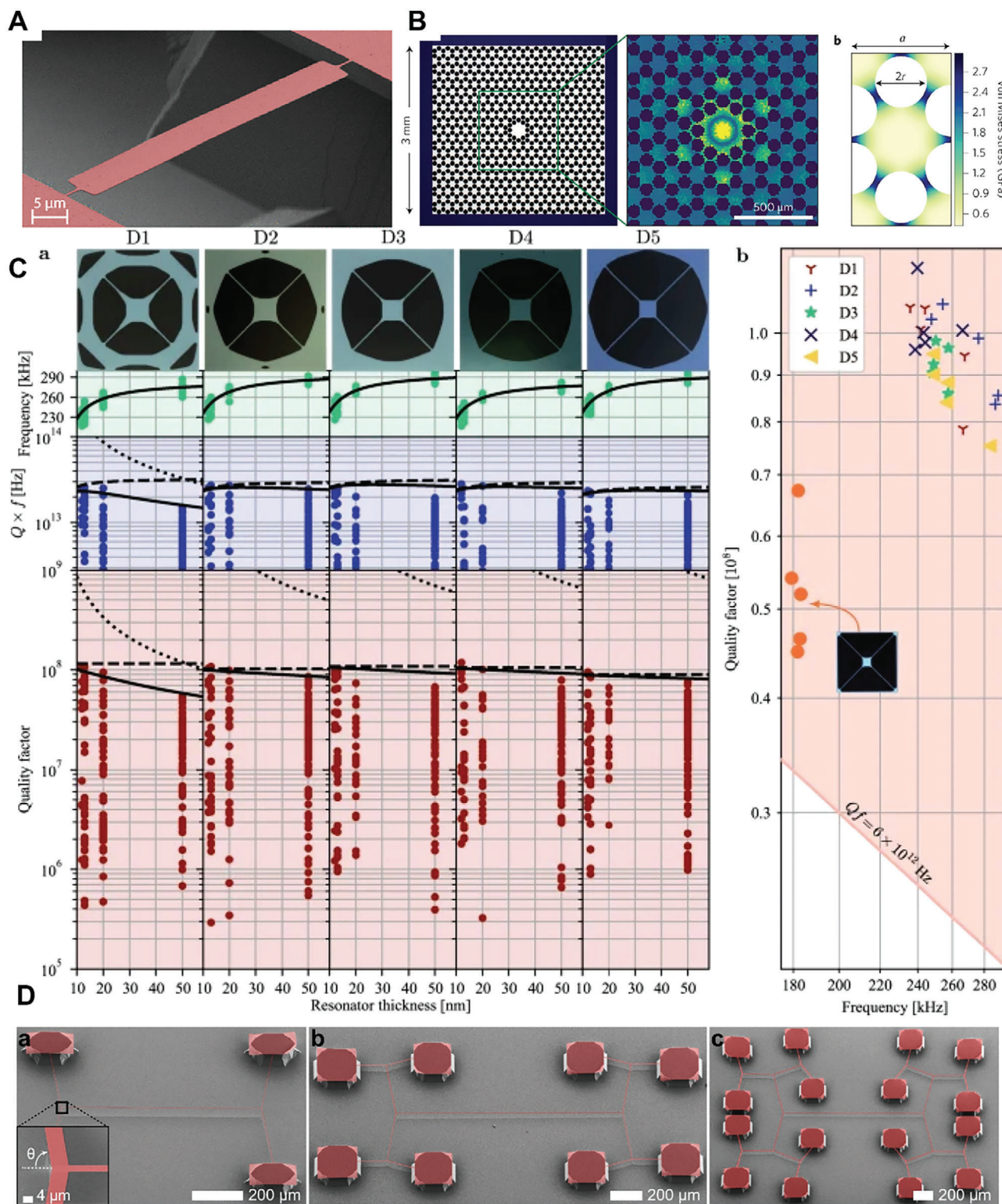


Figure 10. Design of soft clamp geometry. A) Design of clamp-tapering nanobeam. Adapted with permission.^[125] Copyright 2019, American Chemical Society. B) silicon nitride membrane patterned with a photonic crystal structure (left), out-of-plane displacement (middle) and stress distribution (right). Adapted with permission.^[126] Copyright 2017, Springer Nature. C) Topology optimization of structural MMR. Adapted with permission.^[20] Copyright 2021, Springer Nature. D) binary tree beams with varying branching number. Adapted with permission. Copyright 2022, Springer Nature.^[127]

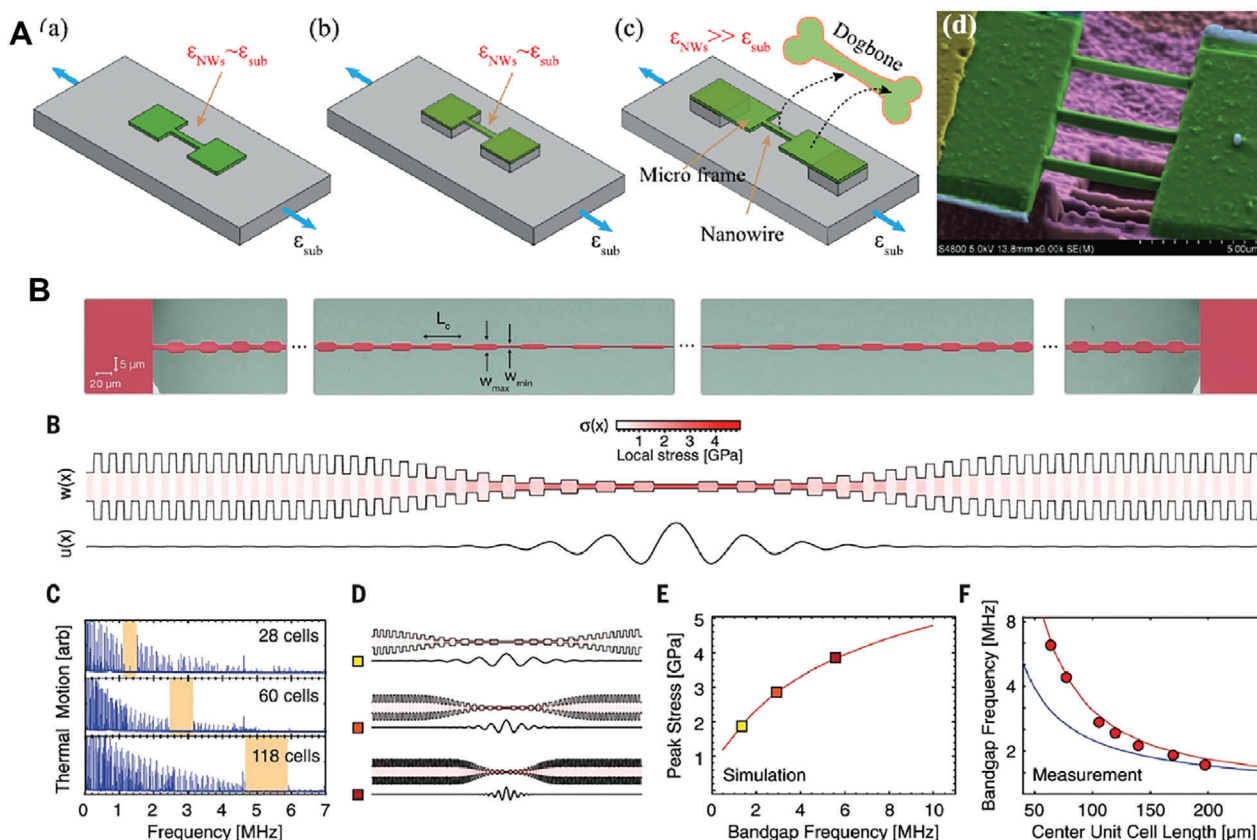


Figure 11. Strain engineering. A) Conventional design of stress concentration in a suspended dogbone structure. Adapted with permission.^[132] Copyright 2016, American Institute of Physics. B) Strain-engineered 1D photonic crystals. Adapted with permission. Copyright 2018, American Association for the Advancement of Science.^[133]

high temperatures and subsequently cooled to room temperature. For example, a residual stress of 1.4 GPa was achieved for 3C-SiC grown on Si(111),^[134] enabling the SiC string resonator to operate at a Q factor of over a million.^[71] However, the current tensile stress induced by material growth is still below the yield strength of the materials, leaving room for future research on stress engineering in MMR sensors to achieve even higher Q factors and performance. Figure 11B illustrates the design of a periodic array (known as phononic crystals) with a tapered width toward the MMR in the middle.^[133] In this case, a residual stress 1 GPa of the Si_3N_4 would result in a high stress concentration of 4 GPa, approaching the yield strength 6 GPa for Si_3N_4 . This design achieved a high-quality factor close to 1 billion and an $f \times Q$ product of 1015. It opens up opportunities for highly sensitive force sensors whose performance depends only on the thermal noise of the surrounding medium. The periodic array is implemented to utilize high-order flexural modes for sufficient stress colocalization, a strategy known as 1D phononic crystals that isolates in-plane flexural modes and keeps them away from clamping points.^[135,136] Additionally, the design of high-Q membrane micro resonators based on 2D phononic crystals has also been demonstrated to suppress radiation losses.^[137] So far, the highest Q factor of 10 billion has been achieved for strained crystalline silicon nanomechanical resonators, thanks to the

combination of low internal friction, high intrinsic strain, and high yield strength.^[59]

Advancements and Challenges: Recent research has generated significant interest in soft clamp geometry and hierarchical structures for strain engineering in high-Q MMR sensors. The appropriate design of soft clamp geometry can minimize energy losses to the substrate and improve quality factors. Strain engineering, with a focus on achieving high stress concentration, is crucial for attaining high-Q factors. The combination of high material quality and substantial strain engineering has resulted in a record-high Q factor of 10 billion, ushering in a new era of opportunities for quantum sensing and transduction.^[59] To achieve even higher Q factors, it is necessary to strain the resonant structure to the upper limit of yield strength, a goal that has not yet been reached for potential materials such as SiC, graphene, diamond, and MXene. Future efforts should aim to find solutions for inducing large stresses (approaching yield strength) in these materials. The achievement of ultrahigh Q factors will drive advancements in quantum sensing applications, including quantum biotechnology.^[138] Anticipating further progress, advanced designs of hierarchical structures utilizing computer-aided design and topology optimization are expected to continue evolving in the coming years. These advances in geometry design will enhance sensing performance and make MMR

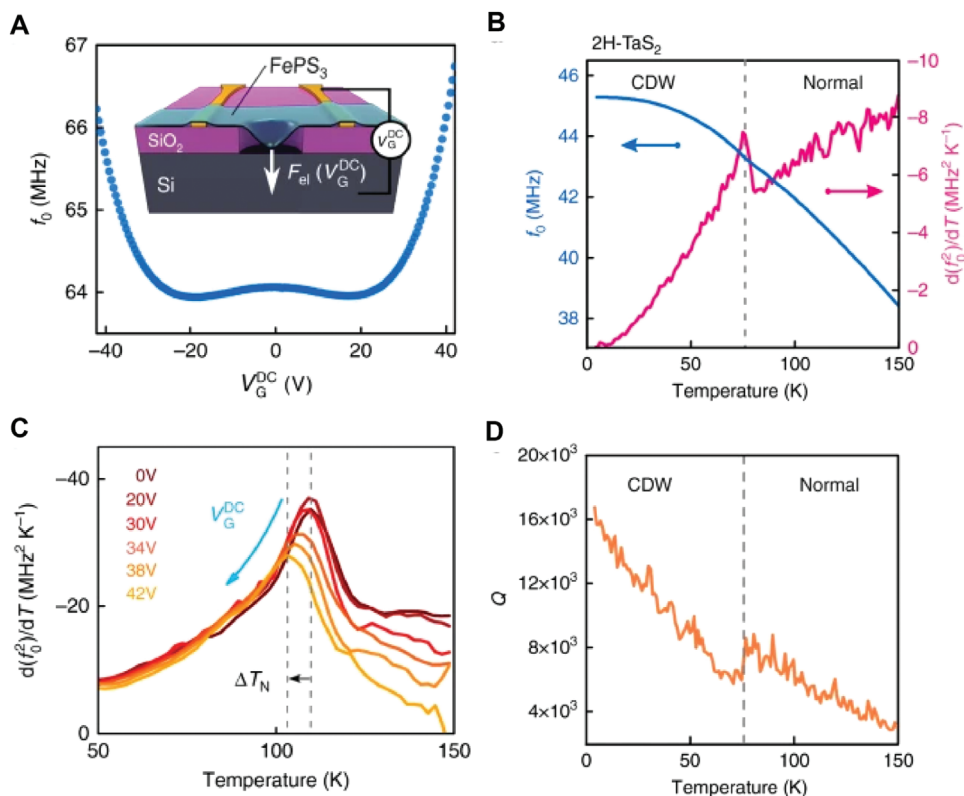


Figure 12. Probing material property by MMR. A) Resonance frequency of FePS3 as a function of gate voltage at 50 K. B) resonant frequency f_0 (solid blue line) and its temperature derivative of $d(f_0^2)/dT$. C) Derivative of f_0^2 as a function of gate voltage and temperature D) Q factor as a function of temperature. Adapted with permission. Copyright 2020, Springer Nature.^[140]

sensors more suitable for a wide range of engineering applications.

5. State-of-the-Art MMR Sensors

MMR sensors have proven to be indispensable tools for characterizing the physical properties of materials. In this section, we will review recent advances in our understanding of new material properties and dynamic phenomena through the measurement of mechanical resonance. Furthermore, we will provide a summary of the recent developments in various types of MMR sensors, including mass, strain, pressure, and thermal sensors.

5.1. Probing Material Properties and Physical Phenomena

The measurement of material properties and physical interactions has led to various discoveries in materials science and physics. For instance, by measuring electronic structures, we gain insights into electronic transport in conducting states of matter, which forms the basis for the development of semiconductor electronics and devices. In the field of MMR sensors, Khivrich et al.^[19] utilized a pump-probe scheme to measure insulating electronic states in a suspended carbon nanotube. This nanotube, vibrating at a frequency of 185 MHz with a Q factor

of 10^4 , enabled the probing of the non-conducting properties of a double quantum dot through frequency shifts and changes in dissipation rate. MMR sensors have also been employed successfully to probe the optical dielectric function of 2D materials.^[139] Šiškins et al.^[140] used temperature-dependent resonance frequency and quality factor to study the phase transition properties of thin membranes of 2D antiferromagnetic FePS3, MnPS3, and NiPS3. **Figure 12A** demonstrates the change in resonant frequency corresponding to the variation of the gate voltage. At an electronic phase transition, the bulk antiferromagnetic material exhibits a charge density wave transition (CDW), which can be detected by anomalies in both the resonant frequency f_0 (solid blue line) and its temperature derivative $d(f_0^2)/dT$, **Figure 12B**. The resonant frequency and Q factor are influenced by both the gate voltage and temperature, as depicted in **Figure 12C** and **Figure 12D**, respectively. MMR sensors have also shed light on the prospect of probing multiple magnetic phase transitions in a single heterostructure, as well as the mechanical and magnetic properties of $\text{Cr}_2\text{Ge}_2\text{Te}_6$, through the observation of magnetoelastic signs dependent on temperature and strain.^[141] Additionally, graphene drums have been utilized to probe the nano motion of single bacteria,^[142] while nanomechanical AFM cantilevers have been employed for rapid detection of bacterial resistance to antibiotics.^[143] Silicon nitride membranes have been employed for high-throughput measurement of signal bacterial cells.^[144] The application of MMR sensors has allowed for a deeper understanding of the magneto-mechanical coupling in 2D

materials, with potential applications in spintronic and nanomagnetic devices.^[141]

In recent years, MMR sensors have proven to be effective tools for investigating a diverse range of dynamical phenomena, including mechanical coupling and coherent motion. For instance, GaAs pillar arrays have shown great potential in elucidating the underlying physics of polarization patterns and topological transport in intricate devices.^[21] Additionally, bulked CNT resonant bridges have been utilized to explore the nonlinear coupling behavior between the in-plane and out-of-plane modes of CNT motion.^[22] Doster et al.^[121] studied the strain-induced strong coupling between two adjacent nanomechanical pillars, highlighting its potential for applications in scanning probe and vectorial force field sensing. Scaling up the system, a network of MMRs can be leveraged to investigate a wide range of collective dynamic behaviors. Furthermore, Stassi et al.^[25] successfully demonstrated weak coupling in a large-scale parallelization of MMR cantilevers, enabling inertial imaging of analytes located far from the sensing MMR cantilever.

Advancements and Challenges: Probing material physics, chemistry, and physical phenomena is essential for advancing our knowledge and unlocking the potential of high-performance sensors and devices. MMR sensors offer unique capabilities and functionalities that enable the characterization of materials and dynamic phenomena, including phase transitions.^[140] The introduction of novel probing methods^[19,140] has expanded our ability to explore previously unexplored properties and phenomena. Moving forward, we expect MMR tools to continue expanding their application range to investigate the properties of various low-dimensional materials, explore mechanical coupling dynamics, and analyze diverse structures. By harnessing the potential of 1D and 2D materials, along with signal processing and advanced electronics, new measurement concepts and advanced sensing techniques can be developed, driving further progress in the field.

5.2. Biological and Chemical Mass Sensors

MMR sensors operate by detecting changes in the effective mass of the MMR structure when it interacts with biological or chemical species. These changes in mass are detected through shifts in the resonant frequency. The extent of frequency shift is determined by various factors, including the geometry (such as dimensions), material type, and the location of the absorbed mass. By analyzing these frequency shifts, MMR sensors provide precise detection of mass changes and enable the characterization of biological and chemical species.^[145]

5.2.1. Single MMR Sensor

Mass sensing with nanoelectromechanical systems (NEMS) has made significant progress in the past decade.^[146–148] Conventional microstructures such as dual-II-BARs^[149] have demonstrated limited sensitivity and mass resolution in the picogram range ($1\text{ pg} = 10^{-12}\text{ g}$). However, recent advancements in nanoscale MMR sensors have shown promising results in probing gaseous analytes and even conducting mass spectrometry on single proteins.^[150] Mass spectrometry allows for rapid identification

of protein species at a small scale. The demand for biological analysis at nanometric scales has driven the need for mass spectrometry with detection capabilities down to the level of single molecules or a few molecules within an individual cell. Various MMR mass sensors have been successfully developed with ultra-high resolutions ranging from femtograms^[151] ($1\text{ fg} = 10^{-15}\text{ g}$), atto-gram^[70] ($1\text{ ag} = 10^{-18}\text{ g}$), zeptogram^[96] ($1\text{ zg} = 10^{-21}\text{ g}$) and even atomic-level resolution^[145] (below 10^{-24} g). **Table 1** provides an overview of the performance of representative nanomechanical resonant mass sensors. For example, **Figure 13A** depicts a nanomechanical mass sensor utilizing a double-walled carbon nanotube (CNT) actuated and sensed electrostatically, **Figure 13B**. This CNT sensor exhibited a mass sensitivity of $1.3 \times 10^{-25}\text{ kgHz}^{-1/2}$ or ≈ 0.40 gold atoms $\text{Hz}^{-1/2}$, **Figure 13C**. In another work, Gil-Santos et al.^[41] demonstrated mass sensing based on the 2D vibration of a nanowire, which exhibited a fundamental flexural vibration mode splitting into two resonance peaks in the x and y directions, **Figure 13D**. In addition to the resonance frequency shifts, the deposition of mass can cause the planes of vibration to rotate.^[41] The rotation angle of the nanowire was found to be dependent on the added mass, **Figure 13E**. The development of MMR sensors is also driving advancements in cell culturing applications, such as characterizing the size and volume of cells.^[52] To achieve highly sensitive mass sensing, resonant sensors require low effective mass and high quality factor (Q). One approach to achieving such high performance is by miniaturizing the resonator size to the nanoscale, thereby reducing the effective mass. The scaling down capability of fabrication technologies plays a crucial role in the performance of MMR sensors for mass detection (**Figure 13F**). Utilizing bottom-up NEMS fabrication techniques is advantageous for achieving high-resolution mass sensing.^[62] However, nanoscale MMR sensors have exhibited non-linear responses and high thermomechanical noise, which limit their dynamic range.^[41,63,70] This also presents challenges such as a small detection area that requires accommodating the analytes within the sensor beam, and high mass resolution often comes at the expense of a reduced capture area.

5.2.2. Inertial Imaging by MMR Array

With an array of many MMR resonance structures on a device, MEMS/NEMS resonant systems provide a sizable sensing area that can be utilized to map the distribution of molecular species and determine the position, shape, and size of adsorbed masses. Maik et al.^[27] demonstrated that the adsorption of analytes results in frequency shifts proportional to the number of adsorbed masses, which can be attributed to several hundred mass adsorption events. When a molecule adsorbs onto the MMR sensor, the mass and position of adsorption can be monitored through the observation of two driven vibrational modes of the structure.^[154] In another work, Hanay et al.^[150] showed that MMR sensors can measure the inertial mass, position of adsorption, size, and shape of individual analytes in real time and at the molecular scale. This allows for achieving a spatial distribution of mass within an individual analyte. The basic principle is based on continuously monitoring the adsorption events of analytes through multimode frequency shifts of the MMR sensors, thereby recording the spatial

Table 1. Representative nanomechanical resonant mass sensors.

Material and structure	Actuation/Sensing	f/Q	Sensitivity & resolution	Refs.
CNT	Electrostatic/ electrostatic	328.5 MHz/1000	1.3×10^{-25} kgHz ^{-1/2}	[145]
D ≈ 2 nm, L = 254 nm				
NEMS bridge	-/magnetomotive	133 and 190 MHz/5000	7 zg	[96]
Si Nanowires	Piezoelectric(mechanical)/optical	2–6 MHz/5–2000	≈50 ag per degree	[41]
D = 5–10 nm and L = 100–300 nm			≈10 pm Hz ^{-1/2} position sensitivity	
CNT	Electrostatic/frequency modulation (FM)	2 GHz/	1.7 yg	[87]
D≈2.2 nm, L ≈ 150 nm				
CNT	Electron beam/SE detector	250 kHz	Zeptogram range	[58]
MoS ₂	Electrostatic/piezoelectric	2400 MHz	3.0×10^{-21} g	[152]
Graphene	Electrostatic/mixing	≈70 MHz/14 000	≈2 zg	[39]
Pillared graphene	–	274–604 GHz	1 yg	[153]

moment of mass distribution for each analyte. The resolution of these sensors strongly relies on the frequency stability.^[150]

Recent advancements in the design of MMR sensors have enabled mass spectrometry to be performed on an array of parallelized cantilevers, allowing for the instantaneous sensing of masses located at significant distances from the sensing cantilever.^[25] Sage et al.^[155] demonstrated mass spectrometry using arrays of 20 multiplexed nanomechanical resonators, each operating at a distinct resonance frequency (Figure 13F). When the frequency jumps exceed the frequency stability of 3σ , the event is counted toward particle identification, enabling the determination of the probability distribution of mass. The number of events was measured for each sensor and plotted on interpolated surface maps. The sensitivity and resolution of MMR sensors are limited by the adsorbed biomolecules, viruses, and analytes, which possess an extremely small mass in the kilodalton (kDa) range ($1 \text{ kDa} = 1.66 \times 10^{-24} \text{ kg}$). The utilization of an aerodynamic lens has proven to be an effective method for improved separation and focusing of nebulized molecules with increasing mass.^[156]

Advancements and Challenges: The use of MMR sensors in biological and chemical applications has garnered significant interest due to their exceptional sensitivity and resolution in measuring mass at the sub-Dalton level.^[96,157] The high-resolution capability of MMR sensors enables the mapping of mass distribution and the characterization of molecular complexes.^[158] However, accurately measuring mass poses challenges as each adsorbed particle or analyte on the MMR structure induces a shift in its resonance frequency, dependent on the adsorption position. This presents difficulties in accurately determining mass. To address this, simultaneous measurement of multiple vibration modes is required, posing further challenges, particularly in practical applications.^[150] It is important to consider the effect of the stiffness change due to mass adsorption that can lead to underestimation of mass.^[41] MMR sensors have not only contributed to mass sensing but have also shed light on the role of mechanical properties in understanding biological processes and pathogenic disorders, including intermolecular interactions and stiffness changes induced by structural alterations in bioanalytes.^[37]

5.3. Force Sensor and Strain Sensors

5.3.1. Force Sensors

Resonant sensors utilize their inertial balance to monitor forces, strain, and stress. They operate based on the principle of frequency shift in response to applied forces and strain. One notable application of resonant force sensing is non-contact atomic force microscopy, which relies on cantilever-based systems.^[159] Further information on force sensing using resonant nanowire cantilevers can be found in^[160] nanomechanical probes such as nanowire,^[161] nanotube^[162] and 2D materials such as graphene^[163] have demonstrated successful applications as highly sensitive force sensors. Figure 14 illustrates an example of SiC nanowire used for force sensing. Recent studies have explored the potential of nanomechanical oscillators, particularly through the analysis of Brownian motion in singly clamped nanowires, for the development of ultrasensitive vectorial force sensing and imaging, achieving sensitivities in the attowatt range.^[164]

Various methods can be employed to enhance the sensitivity of force sensors. Firstly, it is crucial to decouple mechanical motion from the mechanical support and strive for higher quality factors. Additionally, minimizing thermal fluctuations and reducing mechanical damping are essential.^[56,165] Low levels of thermal noise can be achieved by operating at cryogenic temperatures. Successful demonstrations of ultrasensitive nanomechanical force sensing have been achieved in such cryogenic environments.^[161]

In addition, the thermal noise force is determined as follows:^[133]

$$F_{th} = \sqrt{\frac{8\pi k_B T m f}{Q}} \quad (5)$$

To reduce the thermal noise force, it requires design of MMR sensors with small mass, low resonant frequency (e.g., low spring constant) and high quality factors. Several works have focused on scaling down the structures and increasing the

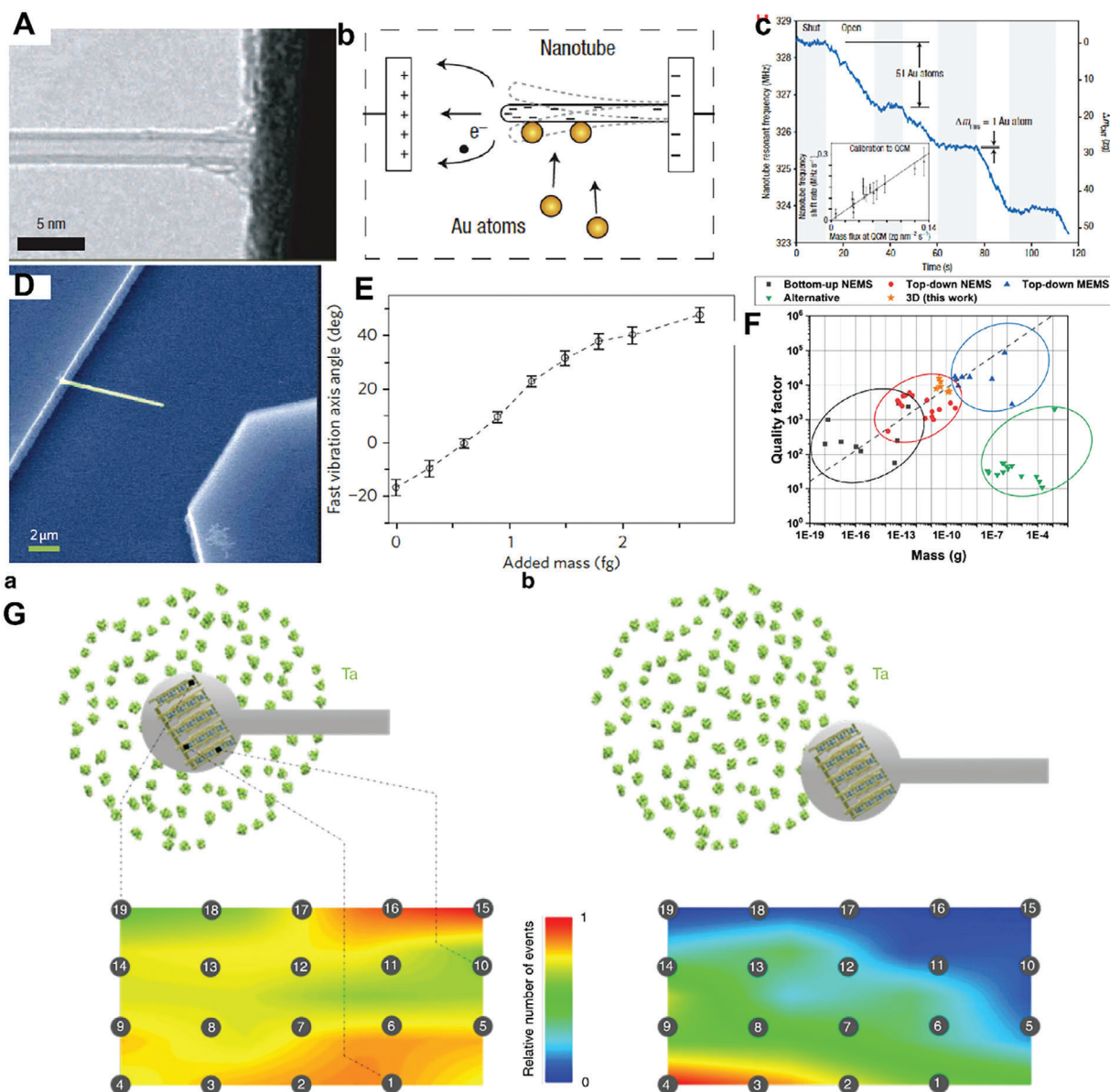


Figure 13. Nanomechanical mass sensing. A) TEM image of a double-walled CNT nanomechanical mass sensor. B) Schematic of actuation and detection of mechanical resonance of CNT. C) The resonant frequency of CNT (left y-axis) and change in adsorbed mass (right y-axis) versus time during evaporation of gold. Adapted with permission.^[145] Copyright 2008, Springer Nature. D) SEM images of a 100-nm-thick nanowire resonant sensors after electron-beam-induced carbon deposition. E) The response of nanowire fast vibration angle to added mass. It is noted that the nanowire vibrates at low and high frequencies referring to slow and fast axes. Adapted with permission.^[41] Copyright 2010, Springer Nature. F) Mass resolution achieved by different fabrication techniques. Adapted with permission.^[62] Copyright 2021, Springer Nature. G) NEMS-mass spectroscopy beam imaging. The array of NEMS sensor is placed at the center of the particle beam (a) or at the edge (b). Adapted with permission. Copyright 2018, Springer Nature.^[155]

quality factors.^[61,162,166] The thermal noise force ranged from $\text{aN}/\text{Hz}^{-1/2}$ to $\text{zN}/\text{Hz}^{-1/2}$ has been achieved for different MMR sensors such as CNT,^[61,162,166] nanowires,^[32,167] graphene,^[163] and others.^[165,168] For example, Figure 14 indicates a very large force sensitivities ($40 \text{ zN}/\text{Hz}^{-1/2}$) with a sensitivity to force field gradients of 20 fN m^{-1} in 40 s ^[161] in SiC nanowires. To date, CNTs have been demonstrated with the lowest level of thermal noise down to $1 \text{ aN Hz}^{-1/2}$.^[166] Compared to 1D structures (nanotubes and nanowires), 2D materials structures have been also demonstrated for force sensing. However, 2D materials exhibited higher

energy losses, resulting in a higher noise level of $\text{fN}/\text{Hz}^{-1/2}$ to $\text{aN}/\text{Hz}^{-1/2}$ or a lower sensitivity.^[163,169]

5.3.2. Strain Sensors

To date, MMR sensors have made less progress in the field of strain sensing, primarily due to their relatively low resolution in the microstrain^[170–172] and nano strain.^[170,173] However, the double-ended tuning fork (DETF) has emerged as a popular

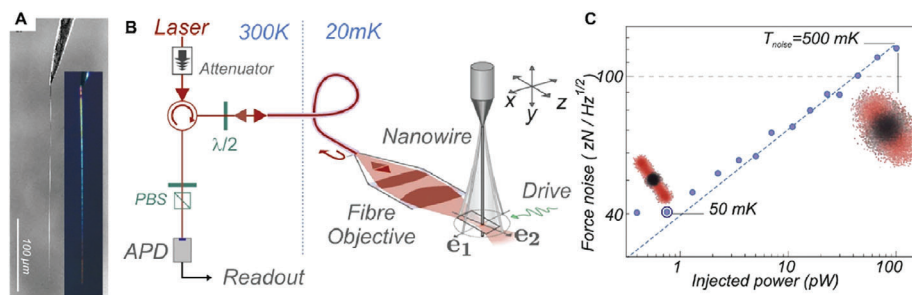


Figure 14. Resonant force sensors. A) SEM and optical images of SiCNWs for ultrasensitive force sensing. B) Sketch of the interferometric readout. Part of the light is reflected on the output face of the fiber and interfere with the light backscattered by the nanowire. C) Dependence of the force noise on optical readout power. Adapted with permission. Copyright 2021, Springer Nature.^[40]

resonant structure for strain detection, thanks to its high sensitivity to strain, ease of design, and characterization.^[170,172] The use of wide bandgap materials, such as SiC, has enabled the demonstration of resonant strain sensors with microstrain resolution, capable of operating in harsh environments, including temperatures above 300 °C and withstanding high shock levels of up to 10 000 g.^[172] Recently, AlN thin films have been used to develop MEMS resonant strain sensors with responsivity (strain sensitivity) of 1700.^[174] Nevertheless, the utilization of nanoscale resonant structures for direct strain sensing remains relatively limited.

5.3.3. Pressure Sensors

Resonant pressure sensors offer superior long-term stability, accuracy, and responsivity compared to non-resonant pressure sensors based on piezoresistive and capacitive mechanisms. These sensors operate by detecting changes in the stiffness of MMR structures when pressure is applied or when surrounding gases are compressed.^[176,177] MMR structures commonly used for pressure sensing include thin membranes^[31] or a nano beams^[152,177,178] supported by a diaphragm. One widely utilized design for pressure sensing is the in-plane double-ended tuning fork (DETF), known for its high-quality factor and low nonlinearity.^[152] Figure 15A–D depicts a graphene pressure sensor with a membrane structure (squeeze-film), demonstrating an increase in resonant frequency with increasing applied pressure. This sensor exhibits a high responsivity of 9 kHz mbar⁻¹, along with reproducible responses and low hysteresis.^[31] Similarly, MoS₂ membrane pressure sensors achieve a pressure responsivity of up to ≈0.77 MHz Torr⁻¹^[179] To enhance the pressure responsivity, the thickness of the pressure-sensing membranes needs to be miniaturized. However, thinner membranes may result in lower quality factors and slower response speeds. Therefore, addressing the trade-off between responsivity and quality factors is crucial for developing high-performance resonant pressure sensors.

Resonant pressure sensors have been a significant focus of research in the field of sensing and actuation. Various methods are employed to enable the operation of resonant pressure sensors, including electrothermal,^[175] electrostatic/capacitive,^[177,180] electromagnetic^[181,182] and optical.^[31] Among these methods, capacitive detection has gained widespread use in pressure sens-

ing devices due to its simplicity of structure implementation and ease of fabrication. However, capacitive detection typically offers relatively low sensitivity, ≈8–10 Hz kPa⁻¹ for silicon resonant pressure sensors,^[183,184] necessitating the use of an amplifier circuit. Piezoresistive detection has also been utilized in pressure sensors, but it requires the integration of piezoresistors into the resonant structures, resulting in complex fabrication processes. However, this method provides higher responsivity compared to capacitive and electromagnetic detections and has the potential for commercialization.^[152,185]

5.3.4. Inertial Sensors

The monitoring of acceleration and angular rotation is essential in a wide range of applications, including navigation (space applications), automotive, and electronics.^[186] Resonant accelerometers offer advantages over non-resonant ones in terms of high accuracy, thanks to direct digital output reading. Resonant accelerometers utilize a resonant beam with a proof mass. When acceleration displaces the position of the proof mass, it induces stress in the resonant structure, altering its stiffness and shifting the resonance frequency accordingly. In Figure 15E, a resonant accelerometer is depicted, featuring a proof mass supported by a resonant beam and excited by an electrothermal signal.^[175] Figure 15F illustrates the shift in resonant frequency in response to applied acceleration. Commercialized micromachined inertial sensors, such as accelerometers, have been well-developed.^[186,187] However, the development of nanoscale inertial sensors is still in its early stages. A high-resolution microchip optomechanical accelerometer was recently demonstrated, offering an acceleration resolution of 10 μg Hz^{-1/2}, low power consumption, large bandwidth (>20 kHz) and a wide dynamic range (>40 dB).^[188] Furthermore, the frequency automatic tracking system (FATS) has been employed to enable static acceleration measurement and expand the synchronization range, enhancing the sensitivity and resolution (1.45 μg) of micromechanical resonant accelerometers.^[189]

Advancements and Challenges: The use of MMR for force and strain sensing has made significant advancements in the past two decades. Achieving high force sensing resolution necessitates minimal noise, which in turn requires MMR structures to resonate at an ultra-high Q factor. MMR has become an indispensable tool in atomic force scanning microscopy, enabling

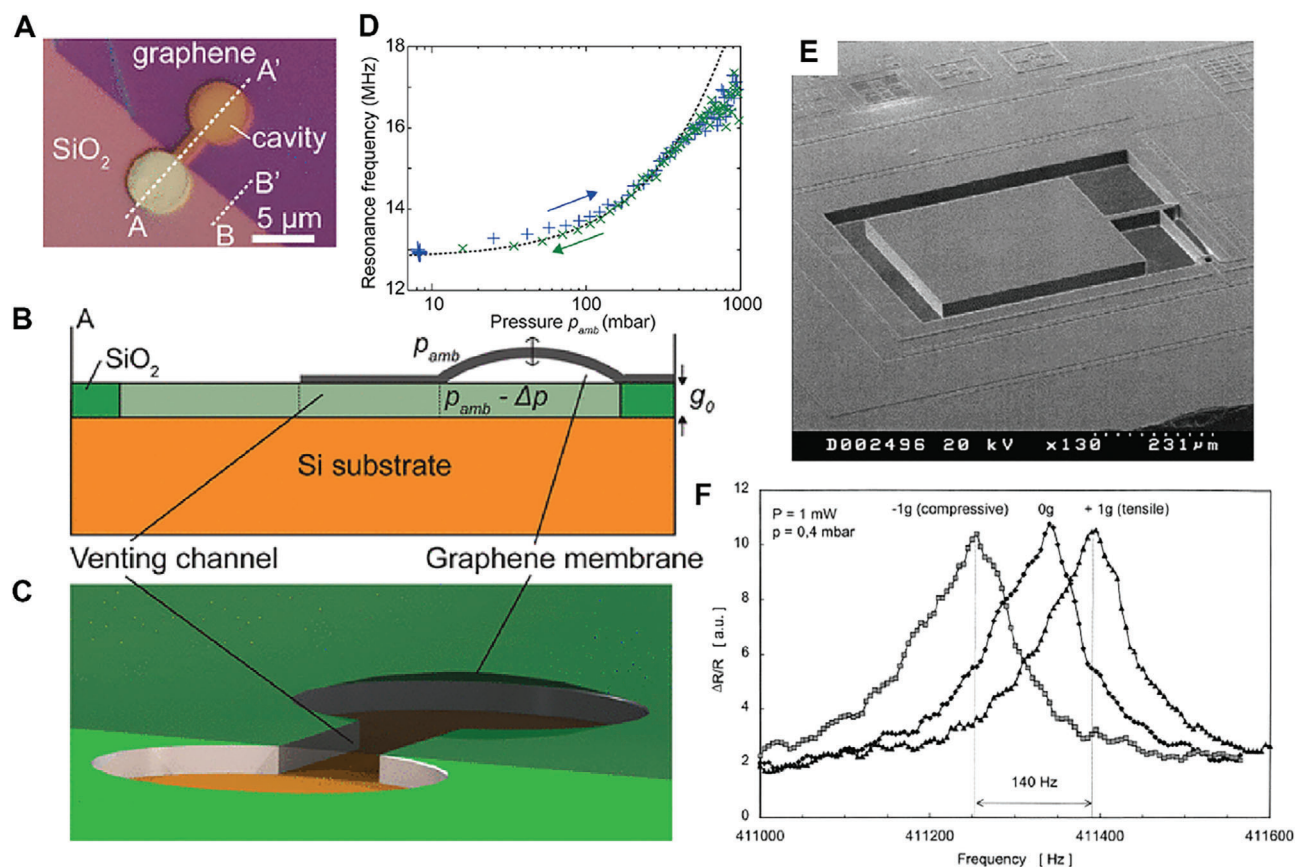


Figure 15. Resonant pressure sensors and accelerometer. A) Graphene flake transferred on a dumbbell shaped hole in a SiO₂ substrate. B) Schematic cross-section of the squeeze-film sensor. C) 3D representation of the squeeze-film sensor design. D) Resonance frequencies as a function of pressure. Adapted with permission.^[31] Copyright 2016, Elsevier. Resonant accelerometer. E) Accelerometer with seismic mass in the center with thermal excitation and piezoresistive readout. F) Measured output signals for different acceleration levels. The sensitivity is 70 Hz g⁻¹. Adapted with permission. Copyright 2001, Elsevier.^[175]

force resolutions in the zeptonewton range and force sensitivities below 1 aNHZ-1.^[61,162,166] The high sensitivity and resolution capabilities of nanomechanical MMR sensors have opened up new frontiers in the detection of electron and nuclear spins, with potential applications in quantum biotechnology.^[138,190] Further enhance detection and performance, deep learning techniques can be employed for data analysis from MMR sensors, including the classification of minimal mass changes.^[191] Higher resolution is associated with higher Q factors, which can be achieved through lower temperature (cryogenic) operation and dissipation dilution techniques. We anticipate that the utilization of new materials and advanced designs, combined with optomechanics, will enable the use of MMR with ultra-high Q factors for force and strain sensing.^[190] Currently, the applications of nanoscale MMR in pressure, strain, and inertial sensing are still under development. The emerging era of space applications with microgravity presents a strong demand for the development of ultrasensitive inertial sensors, in which MMR resonant sensors could be a suitable choice. However, there are challenges to overcome, including the need for low-temperature conditions, measurement interfaces, and the development of chip-level systems that are suitable for practical applications.

5.4. Thermal Sensors

5.4.1. Temperature Sensors

The mechanical properties of materials play a key role in driving the frequency shift and/or quality factor change of resonator structures when subjected to variations in temperature or heat flux. **Figure 16A** illustrates the concept of frequency shifts in nanomechanical structures in response to temperature changes. These temperature variations are induced by applying laser power, resulting in a shift of the resonance frequency.^[139] The sensitivity of thermal sensors is determined by the extent of resonant frequency shift caused by temperature changes as follows.

$$S = TCF = \frac{\Delta f}{f} \times \frac{1}{\Delta T} \quad (6)$$

where TCF is known as the temperature coefficient of frequency. The effect of temperature on the resonant frequency of a material depends on the changes in its modulus of elasticity. Typically, an increase in temperature results in a decrease in the modulus of elasticity, leading to a decrease in the resonant frequency.^[192]

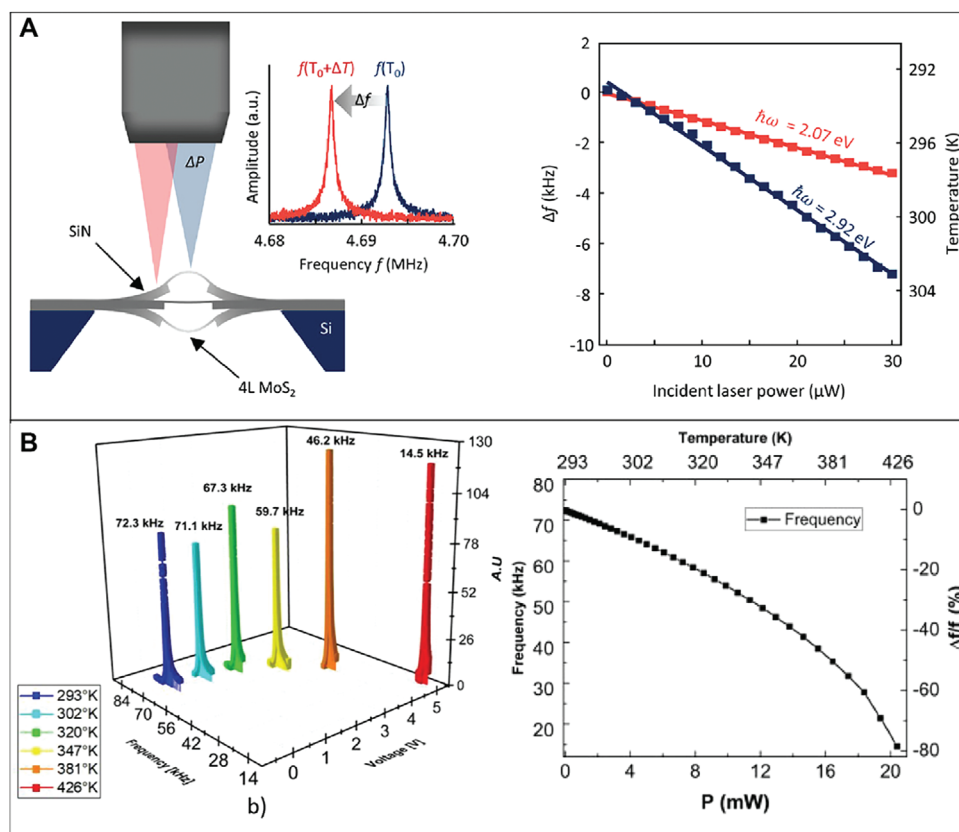


Figure 16. Resonant temperature sensing. A) Temperature sensors based on resonance frequency shift in response to temperature changes. Adapted with permission.^[139] Copyright 2022, American Chemical Society. B) Dependence of resonant frequency on temperature caused by Joule heating of SiC. Adapted with permission. Copyright 2020, Elsevier.^[69]

However, the change in temperature can also introduce tension between the suspended MMR structure and its supporting substrate, resulting in a more complex variation in the resonant frequency.^[69,79] Figure 16B illustrates the temperature dependence of the resonant frequency of SiC under Joule heating, which both softens the structure and affects the residual stress between the suspended SiC and Si substrate. By leveraging the thermal expansion mismatch between the functional layer and its substrate, high temperature sensitivity has been achieved, such as $-1.74\%/K$ for silicon nitride and aluminium micro strings.^[193] The concept of resonant temperature sensing has garnered significant interest in both research and commercial applications, particularly in resonant thermometers. For example, resonant quartz-based temperature sensors with a temperature resolution as high as 0.1 mK (e.g., Hewlett Packard 2804A Quartz Thermometer) have been available on the market. However, the development of quartz-based resonant thermal sensors has encountered challenges in terms of miniaturization and integration.

Temperature changes can also be assessed by observing the corresponding changes in quality factors, which are indicative of thermoelastic losses.^[194] However, relying solely on the temperature-dependent quality factor (Q factor) is not preferred due to the significant impact of the viscous damping effect in air conditions. Environmental factors can significantly degrade the performance of resonant thermal sensors. For instance, studies have demonstrated the strong influence of humidity on the

performance of such sensors.^[195–197] Furthermore, resonant temperature sensors have recently been successfully demonstrated for harsh environments.^[198] The resonant structure based on AlScN-on-SiC thin film exhibited excellent stability to temperature variations for the first vibration mode, while larger temperature coefficient of frequency (TCF) values were measured at higher modes, indicating the potential for sensitive temperature sensing in harsh environments.^[198] The development of such sensors is expected to continue addressing the challenges posed by space applications in the coming years. Shape memory polymer resonant sensors have also been demonstrated, showcasing unprecedented high sensitivity of $1.2\%/K$.^[199] This sensitivity is comparable to graphene temperature sensors^[72,183] and exceeds that of other 2D materials such as MoS_2 ($-0.396\%/K$)^[200] and h-BN ($-0.285\%/K$).^[120] Table provides an overview of the performance of several representative nanomechanical resonant thermal sensors (Table 2).

5.4.2. Infrared (IR) Sensors

Infrared sensing technologies have found wide-ranging applications, including missile tracking, surveillance, medical diagnostics, and thermal imaging. Conventional infrared sensing relies on the interaction between photons (light) and electrons in semiconductors to generate electrical output, known as a photon

Table 2. Representative nanomechanical resonant thermal sensors.

Material and structure	Actuation/Sensing	f/Q	Sensitivity and resolution	Ref.
Si torsion paddle	Piezo-disk/optical (laser)	≈1 MHz/913	Flexural TCF = 548 ppm K ⁻¹ Torsional TCF = 92 ppm K ⁻¹	[28]
Si ₃ N ₄ on SiO ₂ tuning fork	–/Near-field optical readout	16.51 MHz/–	TCF = 2.5 and 182 ppm K ⁻¹	[201]
Phase change polymer	Piezodisk/optical (laser doppler)	10–20 kHz/ 1–40	0.4–1.2%K ⁻¹	[199]
Graphene-AlN	Piezoelectric/optical	225–307 MHz/	TCF = –29.4 to –26.9 ppm K ⁻¹	[202]
AlN contour-mode rectangular plate resonator	Piezoelectric/electrical	19 to 656 MHz/	TCF = –25 ppm K ⁻¹	[203]
GaN resonator	–	2.18 GHz/655	TCF = –18 ppm K ⁻¹	[204]
Y-cut-quartz bulk acoustic wave resonator	–	241 MHz/4200	TCF = 92 ppm K ⁻¹	[205]
Lithium niobate (LN) based MEMS resonators	–	273 MHz/1860	TCF = –80 ppm K ⁻¹	[206]

detector. However, this method requires cryogenic cooling, resulting in bulky and expensive systems. Another type of IR sensing is based on the electrical properties change of materials,^[207] which does not require cryogenic cooling but exhibits low sensitivity and slow response time. Resonant infrared sensing, on the other hand, operates at room temperature and offers several advantages over non-resonant methods, such as low-noise performance due to high quality factor, high accuracy, and simple conversion to digital signals by measuring zero crossings.^[18,208] To detect an infrared signal, infrared absorbers need to be integrated on top of resonant structures. These absorbers consist of thin layers of materials, such as dielectrics, which can absorb infrared wavelengths and convert them into thermal energy. **Figure 17A** illustrates the schematic of a torsional IR bolometer, featuring a torsional paddle coated with a nanometer-thick TiN film as the absorbing material. This bolometer demonstrated an uncooled noise equivalent temperature difference of 390 mK.^[202] When the MMR bolometer absorbs light, the temperature of the structure increases, leading to thermomechanical stress and a shift (Δf_0) in the resonance frequency according to the equation:^[42,209]

$$\Delta f_0 = \frac{\alpha E f_0}{2\sigma_0 (1 - \nu)} \Delta T \quad (7)$$

where α , ν and E are the thermal expansion coefficient, the Poisson ratio and the Young's modulus, respectively; σ_0 is the alternating thermal stress that can be utilised to enhance the IR radiation sensitivity.

Apart from the Temperature Coefficient of Frequency (TCF), another important figure of merit for IR sensors is the Noise Equivalent Differential Temperature (NEDT), defined as $NEDT = \Delta T/SNR$, where ΔT and SNR are the temperature change at the target and signal-to-noise ratio, respectively. To enhance IR sensitivity, it is crucial to select absorbers with high spectral wavelength absorptance and thermal resistance to minimize thermal losses. **Figure 17B** demonstrates a significant improvement (13 times) in IR responsivity of graphene-AlN NEMS resonators compared to a reference device using Au as the top

electrode,^[202] attributed to the enhanced infrared absorptance of graphene-AlN.

Additionally, another approach for achieving ultrasensitive infrared detection involves increasing the TCF by utilizing a material with a strong dependence of its Young's modulus on temperature. For instance, a shape memory polymer (SMP) has been successfully demonstrated with a TCF of 8%K⁻¹ at a phase-change temperature of 45 °C which is two orders of magnitude higher than conventional IR resonant sensors,^[199] **Figure 17C**.

Low noise levels are crucial for the development of sensitive IR sensors. Conventional microbolometers and commercial devices typically exhibit room-temperature noise-equivalent powers in the range of ≈100 pW Hz^{-1/2}.^[47] **Figure 17D** showcases a recently developed graphene bolometer, presenting its design, images, and mechanical properties of the graphene MMR resonance structure. This bolometer operates at room temperature and offers high speed and sensitivity (noise-equivalent power of 2 pW Hz^{-1/2}) along with a wide bandwidth ranging from 10 kHz up to 1.3 MHz. These exceptional performance characteristics are attributed to the unique properties of graphene, including its low mass per unit area, high thermal stability, and exceptional spectral absorptance.^[42]

It's worth noting that MMR bolometers face a trade-off between speed and sensitivity due to the inverse relationship between heat capacity and response time. To achieve high-speed detection, 1D and 2D materials are favorable options due to their atomic thin structures.^[42,208]

Advancements and Challenges: Resonant nanomechanical thermal systems have made remarkable progress in recent years, eliminating the need for cryogenic temperature conditions. Some current research focuses on temperature and infrared sensing in combination with other sensing effects to estimate material properties.^[210] Materials such as graphene and GaN, known for their thermal stability and ease of fabrication, hold great potential for MMR-based high-temperature sensing applications.^[42,211] We expect that further optimization of MMR geometry, combined with strain engineering techniques, will be pursued to achieve enhanced temperature and infrared sensitivity.

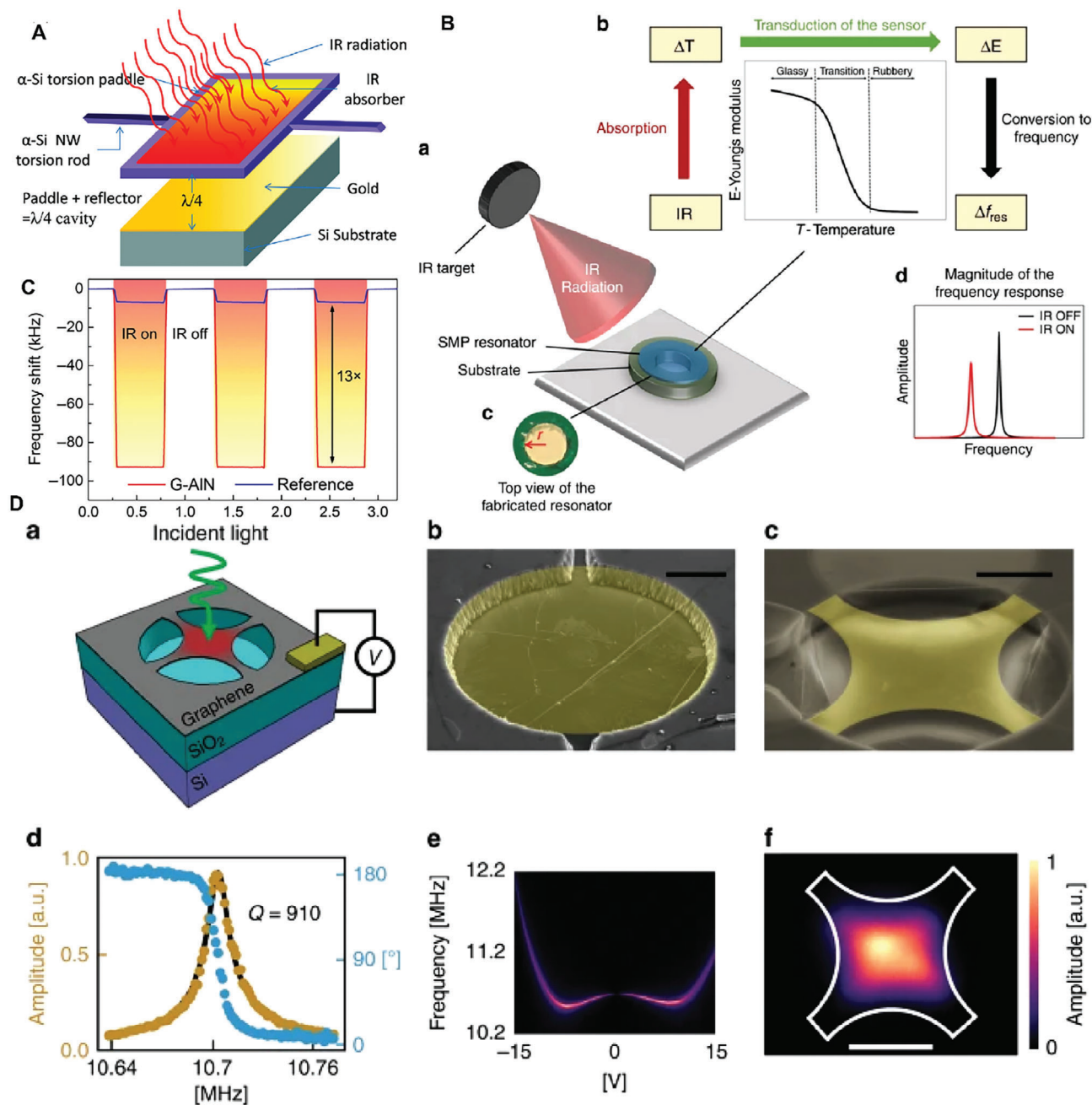


Figure 17. Thermal sensing. A) Schematic layout of a torsional-frequency-shift-based Si IR detector with torsional and flexure modes. Adapted with permission.^[28] Copyright 2013, American Chemical Society. B) Frequency shift of graphene–aluminium nitride resonant infrared detector with IR irradiation. Adapted with permission.^[202] Copyright 2016, Springer Nature. C) IR thermal resonant sensor system. D) Working principle of thermal resonant sensor. E) Top view of a shape memory polymer resonator for thermal sensing. F) The frequency response of thermal resonant sensor. Adapted with permission.^[199] Copyright 2019, Springer Nature. G) graphene nanomechanical bolometer (GNB) which comprises a suspended graphene membrane. Adapted with permission. Copyright 2019, Springer Nature.^[42]

To improve resolution and sensitivity, it is important to enhance the optical/thermal absorption capability of MMR. One possible solution is to deposit a new effective absorptive material on the MMR structure. However, there exists a trade-off between sensitivity and bandwidth/speed of detection, which requires further exploration in the future.

Another challenge lies in achieving uniformity in MMR structure arrays and scalable production, especially when working with new 2D materials. Packaging and electronic integration, along with on-chip actuation and detection, will play a crucial role in advancing the commercialization of MMR thermal sensors.

5.5. Other Sensors

The monitoring of fluid characteristics plays a crucial role in controlling industrial processes across various applications, including food and automotive manufacturing. MMR sensors offer a means to determine viscosity, density, and other physical properties of fluids and environments by measuring the shift in resonant frequency or quality factor.^[212,213]

For example, conventional cantilever-based MMR sensors exhibit a resonant frequency that depends on density, while their quality factor is influenced by viscosity. The change in the resonant frequency has been utilized to develop gas and humidity sensors.^[214,215] Recently, by scaling down the thickness to ≈ 200 nm, zinc oxide resonant microcantilevers have been successfully demonstrated for ultrasensitive humidity sensor with a sensitivity of 23 649 ppm/% RH at 5.8% RH.^[216] In many cases, the resonant characteristics of MMR sensors have been found to be dependent on the product of liquid density and viscosity,^[217] as well as the vibration modes.^[212,213] Higher-order resonant frequencies generally correspond to higher quality factors, thereby improving the accuracy of density and viscosity measurements.^[218]

To enhance measurement accuracy, MMR sensors are typically driven to oscillation, allowing precise tracking of the amplitude peak.^[219] For example, Manzanque et. al. demonstrated a piezoelectric oscillator with a minimum detection limit of 4.09×10^{-6} g mL⁻¹ for the density and 2.07×10^{-3} mPa s for the viscosity.^[220] MMR sensors have also been utilized to monitor changes in sugar and ethanol concentrations with a resolution of 1 mg mL⁻¹ and 20 μ Pa s for density and viscosity, respectively.^[221] Recently, piezoelectric-AlN MMR sensors operating in 2D flexural modes have shown promise in decoupled measurements of density and viscosity for fluid property monitoring.^[222] n-plane vibration modes with shear force applied to MMR are preferred for achieving higher quality factors compared to flexural modes, which are influenced by compressive forces.^[223]

In addition to direct measurement of fluid characteristics, it is important to note that MMR sensors operating in high-density and high-viscosity environments may experience a low quality factor due to damping effects, leading to significant energy losses to the surroundings.^[224–226] This poses the challenge when monitoring other parameters in liquid operating environments.

Another type of sensor utilized for charge perturbation measurement is the electrometer. MMR sensors have been employed to detect and quantify the mechanical vibration-induced generation and transport of charge in resonance structures. The principle of charge detection based on mechanical resonance relies on tracking the shifts in resonant frequency of MMR structures as they respond to changes in charge.^[227] For example, nanomechanical torsional beam structures have been successfully used to measure variations in charge, resulting in shifts in the resonance frequency of the beams.^[228] Another effective configuration is the clamped-clamped beam, which offers the advantage of low noise levels when detecting electric charges.^[229] The suspended capacitor, consisting of an array of interdigitated electrodes, is widely employed as a basic structure for charge sensing.^[227] Additionally, 2D materials like MoS₂ have demonstrated electrometer capabilities with impressive charge resolutions of below 10 electrons.^[230] Similarly, 1D materials such as carbon nanotubes

(CNTs) have exhibited a strong coherence between mechanical motion and charge fluctuations, indicating their potential for electron tuning and detection.^[76]

6. Conclusion and Future Perspectives

The utilization of MMR devices, particularly nanomechanical resonant sensors, has made remarkable progress in biological, chemical, and physical sensing applications. A key focus of development in this field is the miniaturization or scaling down of structures to the nanometric and atomic scale. This endeavor aims to achieve ultralow effective mass (as low as one Dalton Da or atomic mass unit), ultra-high frequency operation (in the GHz range), and ultra-high quality factor (up to 10 billion). These characteristics contribute to high sensitivity, resolution, and detection speed. Recent advancements in resonant sensing have expanded its capabilities to high-temperature and harsh environment sensing, as well as quantum sensing. Notably, resonant sensing applications, including mass sensing, have garnered significant interest and achieved unprecedented levels of performance.

In the future, there is a need for further development of advanced MMR sensors for detecting physical signals such as temperature, infrared, pressure, and inertial sensing. However, a major challenge lies in miniaturizing resonance structures to the nanometric or atomic scale while enabling large-scale production. Fabrication of nanoscale suspended arrays, especially for 2D materials, remains challenging, particularly at the wafer-scale production level. Scaling down to the nanometric/atomic scale also poses challenges in detecting mechanical motion and signal processing. The surrounding environment's impact on the mechanical motion of nanoscale resonant sensors is significant, potentially leading to underestimated measurement results. Given their high surface-to-volume ratio and low mass, nanoscale MMR sensors are highly sensitive to perturbations. Achieving a high quality factor and sensitivity typically requires cryogenic temperatures, which limits the practical applications of MMR sensors.

Based on our review, we believe that the future development of MMR sensors could benefit from the following active research directions:

- The development of biological, chemical and physical MMR sensors should be continued in the future. While MMR sensors based on conventional semiconductors (Si, GaN, etc.), carbon nanotubes and 2D materials (graphene, MoS₂, etc.) have been successfully demonstrated for sensing, new materials such as MXene would be potential to be explored further for new sensing functions thanks to their excellent mechanical properties.
- Scaling down the size of MMR sensors will require to go with integration capability, scalable fabrication and uniformity of devices. To pursue this, alternative fabrication methods such as additive manufacturing would also be of interest to achieve comparable sensing performance with conventional fabrication techniques. More studies need to carry out to understand the interaction between surface of MMR sensors with testing sample and environments to achieve accurate measurement of measurands.
- Ultra-high Q factor and high figure of merit are of considerable interest toward quantum sensing capability. We expect that

near-zero Kelvin temperature, optimized designs and strain engineering continue to be employed to achieve dissipation dilution and minimize energy losses. Optimal topology designs are expected to contribute to this goal. The improvement of high-quality materials such as high crystalline morphologies reduces the internal losses during mechanical vibration, which would significantly contribute to future advances of ultra-high Q MMR sensors.

- Methods of detection need advancements toward high reliability of detecting small signals and integration for practical applications. In this aspect, both the excitation and the detection by electrical signals will create pathways for on-chip detection.
- MMR sensors can be utilized to probe interesting new materials properties and dynamic phenomena such as phase transition. To realize this function, different effective measurement strategies need to be established for MMR sensors.
- Resonant sensors utilized for harsh environments would receive much more attention to provide a reliable tool for probing signals in space applications. Development of MMR sensors based on wide band gap materials is expected thanks to the excellent thermal stability and unique properties for hostile conditions.
- Multifunctional and multimodal resonance sensing have been hardly found. Most current MMR sensors aim to detect a signal quantity such as mass and temperature. To realize multifunctional and multimodal sensing, decoupling of signals from multiple inputs will be a challenge to be addressed.
- For practical applications, the signals captured from any MMR sensor array can be analyzed in combination with artificial intelligence (AI), machine learning or deep learning models, depending on availability of data to predict the patterns, activities and incidents in several, diverse emerging high-tech biological and medical applications. Using pattern analysis or classification algorithms, for example, can assist in improving diagnostics and therapeutic accuracy in the nanotechnology field. In nanomedicine, artificial intelligence techniques may be used to optimize material properties by predicting their link with the target medicine, as well as biological fluids and cell membranes that influence therapeutic drug efficacy. In addition, AI-powered meta surface-based resonant biosensors could be developed to investigate inherently complex biological processes. Among these are exosomes which facilitate intercellular communication and nucleic acid and carbohydrate interactions, as well as proteins involved in gene regulation or neurodegeneration in biology, bio-analytics, and pharmacology, as well as basic research and disease diagnostics and drug development in medicine.

Acknowledgements

The research was funded by the Australian Research Council through grants DE210100852 and DP240102230.

Open access publishing facilitated by University of Southern Queensland, as part of the Wiley - University of Southern Queensland agreement via the Council of Australian University Librarians.

Conflict of Interest

The authors declare no conflict of interest.

Keywords

micromechanical systems, nanomechanical systems, quality factors, resonant frequencies, resonant sensors, resonators

Received: June 6, 2023
Revised: October 26, 2023
Published online: December 14, 2023

- [1] E. A. Laird, F. Pei, W. Tang, G. A. Steele, L. P. Kouwenhoven, *Nano Lett.* **2012**, *12*, 193.
- [2] M. Jung, P. Rickhaus, S. Zihlmann, A. Eichler, P. Makk, C. Schönenberger, *Nanoscale* **2019**, *11*, 4355.
- [3] K. Eom, H. S. Park, D. S. Yoon, T. Kwon, *Physics Reports* **2011**, *503*, 115.
- [4] S. S. Verbridge, H. G. Craighead, J. M. Parpia, *Appl. Phys. Lett.* **2008**, *92*, 013112.
- [5] S. S. Verbridge, J. M. Parpia, R. B. Reichenbach, L. M. Bellan, H. G. Craighead, *J. Appl. Phys.* **2006**, *99*, 124304.
- [6] A. I. Fedorchenko, I. Stachiv, W.-C. Wang, *Flow Meas. Instrum.* **2013**, *32*, 84.
- [7] S. Schmid, K. Jensen, K. Nielsen, A. Boisen, *Phys. Rev. B* **2011**, *84*, 165307.
- [8] J. Tamayo, P. M. Kosaka, J. J. Ruz, Á. S. Paulo, M. Calleja, *Chem. Soc. Rev.* **2013**, *42*, 1287.
- [9] A. H. Safavi-Naeini, J. Chan, J. T. Hill, T. P. M. Alegre, A. Krause, O. Painter, *Phys. Rev. Lett.* **2012**, *108*, 033602.
- [10] F. Pistolesi, A. Cleland, A. Bachtold, *Phys. Rev. X* **2021**, *11* 031027.
- [11] A. Baydin, F. Tay, J. Fan, M. Manjappa, W. Gao, J. Kono, *Materials* **2022**, *15*, 1535.
- [12] S. Kolkowitz, A. C. Bleszynski Jayich, Q. P. Unterreithmeier, S. D. Bennett, P. Rabl, J. Harris, M. D. Lukin, *Science* **2012**, *335*, 1603.
- [13] A. J. Heinrich, W. D. Oliver, L. M. Vandersypen, A. Ardavan, R. Sessoli, D. Loss, A. B. Jayich, J. Fernandez-Rossier, A. Laucht, A. Morello, *Nat. Nanotechnol.* **2021**, *16*, 1318.
- [14] E. E. Wollman, C. Lei, A. Weinstein, J. Suh, A. Kronwald, F. Marquardt, A. A. Clerk, K. Schwab, *Science* **2015**, *349*, 952.
- [15] P. Enoksson, G. Stemme, E. Stemme, *J. Microelectromech. Syst.* **1997**, *6*, 119.
- [16] Y. Tao, J. M. Boss, B. Moores, C. L. Degen, *Nat. Commun.* **2014**, *5*, 1.
- [17] U. E. Ali, G. Modi, R. Agarwal, H. Bhaskaran, *Nat. Commun.* **2022**, *13*, 1.
- [18] G. Stemme, *J. Micromech. Microeng.* **1991**, *1*, 113.
- [19] I. Khivrich, A. A. Clerk, S. Ilani, *Nat. Nanotechnol.* **2019**, *14*, 161.
- [20] D. Høj, F. Wang, W. Gao, U. B. Hoff, O. Sigmund, U. L. Andersen, *Nat. Commun.* **2021**, *12*, 1.
- [21] J. Doster, T. Shah, T. Fösel, P. Paulitschke, F. Marquardt, E. M. Weig, *Nat. Commun.* **2022**, *13*, 1.
- [22] S. Rechnitz, T. Tabachnik, M. Shlafman, S. Shlafman, Y. E. Yaish, *Nat. Commun.* **2022**, *13*, 1.
- [23] X. Zhang, K. Makles, L. Colombier, D. Metten, H. Majjad, P. Verlot, S. Berciaud, *Nat. Commun.* **2020**, *11*, 1.
- [24] X. Meng, H. Zhang, J. Song, X. Fan, L. Sun, H. Xie, *Nat. Commun.* **2017**, *8*, 1.
- [25] S. Stassi, G. De Laurentis, D. Chakraborty, K. Bejtka, A. Chiodoni, J. E. Sader, C. Ricciardi, *Nat. Commun.* **2019**, *10*, 1.
- [26] N. M. M. Pires, T. Dong, U. Hanke, N. Hoivik, *Sensors* **2014**, *14*, 15458.
- [27] A. K. Naik, M. Hanay, W. Hiebert, X. Feng, M. L. Roukes, *Nat. Nanotechnol.* **2009**, *4*, 445.
- [28] X. Zhang, E. Myers, J. Sader, M. Roukes, *Nano Lett.* **2013**, *13*, 1528.

- [29] V. J. Gokhale, M. Rais-Zadeh, *J. Microelectromech. Syst.* **2013**, *23*, 803.
- [30] M. Moosavifar, A. Ansari, M. Rais-Zadeh, *IEEE SENSORS* **2016**, 1.
- [31] R. J. Dolleman, D. Davidovikj, S. J. Cartamil-Bueno, H. S. van der Zant, P. G. Steeneken, *Nano Lett.* **2016**, *16*, 568.
- [32] N. Rossi, F. R. Braakman, D. Cadeddu, D. Vasyukov, G. Tütüncüoğlu, A. Fontcuberta i Morral, M. Poggio, *Nat. Nanotechnol.* **2017**, *12*, 150.
- [33] R. Abdolvand, B. Bahreyni, J. E.-Y. Lee, F. Nabki, *Micromachines* **2016**, *7*, 160.
- [34] W. P. Eaton, J. H. Smith, *Smart Mater. Struct.* **1997**, *6*, 530.
- [35] N. Ghaemi, A. Nikoobin, M. R. Ashory, *Adv. Electron. Mater.* **2022**, 2200229.
- [36] B. Arash, J.-W. Jiang, T. Rabczuk, *Appl. Phys. Rev.* **2015**, *2*, 021301.
- [37] M. Calleja, P. M. Kosaka, Á. S. Paulo, J. Tamayo, *Nanoscale* **2012**, *4*, 4925.
- [38] B. Xu, P. Zhang, J. Zhu, Z. Liu, A. Eichler, X.-Q. Zheng, J. Lee, A. Dash, S. More, S. Wu, *ACS Nano* **2022**.
- [39] C. Chen, S. Rosenblatt, K. I. Bolotin, W. Kalb, P. Kim, I. Kymissis, H. L. Stormer, T. F. Heinz, J. Hone, *Nat. Nanotechnol.* **2009**, *4*, 861.
- [40] F. Fogliano, B. Besga, A. Reigue, L. Mercier de Lépinay, P. Heringlake, C. Gouriou, E. Eyraud, W. Wernsdorfer, B. Pigeau, O. Arcizet, *Nat. Commun.* **2021**, *12*, 1.
- [41] E. Gil-Santos, D. Ramos, J. Martínez, M. Fernández-Regúlez, R. García, Á. San Paulo, M. Calleja, J. Tamayo, *Nat. Nanotechnol.* **2010**, *5*, 641.
- [42] A. Blaikie, D. Miller, B. J. Alemán, *Nat. Commun.* **2019**, *10*, 1.
- [43] Y. Bao, P. Xu, S. Cai, H. Yu, X. Li, *Talanta* **2018**, *182*, 148.
- [44] J. Henriksson, L. G. Villanueva, J. Brugger, *Nanoscale* **2012**, *4*, 5059.
- [45] T. Nguyen, T. Dinh, H.-P. Phan, T.-K. Nguyen, A. P. Joy, B. Bahreyni, A. Qamar, M. Rais-Zadeh, D. G. Senesky, N.-T. Nguyen, *Nano Energy* **2020**, *76*, 104950.
- [46] D. Davidovikj, P. H. Scheepers, H. S. Van Der Zant, P. G. Steeneken, *ACS Appl. Mater. Interfaces* **2017**, *9*, 43205.
- [47] L. Vicarelli, A. Tredicucci, A. Pitanti, *ACS Photonics* **2022**, *9*, 360.
- [48] Z. Wang, J. Lee, P. X.-L. Feng, *Nat. Commun.* **2014**, *5*, 5158.
- [49] A. Rahafrooz, S. Pourkamali, *IEEE Trans. Electron Devices* **2011**, *58*, 1205.
- [50] A. Rahafrooz, S. Pourkamali, *J. Micromech. Microeng.* **2010**, *20*, 125018.
- [51] D. Alsteens, Y. F. Dufrêne, *Nature* **2017**, *550*, 465.
- [52] D. Martínez-Martín, G. Fläschner, B. Gaub, S. Martin, R. Newton, C. Beerli, J. Mercer, C. Gerber, D. J. Müller, *Nature* **2017**, *550*, 500.
- [53] L. Sementilli, E. Romero, W. P. Bowen, *Adv. Funct. Mater.* **2022**, *32*, 2105247.
- [54] C. Zener, *Phys. Rev.* **1938**, *53*, 90.
- [55] S. Galliou, M. Goryachev, R. Bourquin, P. Abbé, J. P. Aubry, M. E. Tobar, *Sci. Rep.* **2013**, *3*, 2132.
- [56] H. Mamin, D. Rugar, *Appl. Phys. Lett.* **2001**, *79*, 3358.
- [57] K. Waszczuk, T. Piasecki, K. Nitsch, T. Gotszalk, *Sens. Actuators, B* **2011**, *160*, 517.
- [58] G. Gruber, C. Urgell, A. Tavernarakis, A. Stavrinadis, S. Tepsic, C. Magén, S. Sangiao, J. De Teresa, P. Verlot, A. Bachtold, *Nano Lett.* **2019**, *19*, 6987.
- [59] A. Beccari, D. A. Visani, S. A. Fedorov, M. J. Beryehi, V. Boureau, N. J. Engelsens, T. J. Kippenberg, *Nat. Phys.* **2022**, *18*, 436.
- [60] J. M. L. Miller, A. Ansari, D. B. Heinz, Y. Chen, I. B. Flader, D. D. Shin, L. G. Villanueva, T. W. Kenny, *Appl. Phys. Rev.* **2018**, *5*, 041307.
- [61] S. De Bonis, C. Urgell, W. Yang, C. Samanta, A. Noury, J. Vergara-Cruz, Q. Dong, Y. Jin, A. Bachtold, *Nano Lett.* **2018**, *18*, 5324.
- [62] S. Stassi, I. Cooperstein, M. Tortello, C. F. Pirri, S. Magdassi, C. Ricciardi, *Nat. Commun.* **2021**, *12*, 1.
- [63] H. C. Postma, I. Kozinsky, A. Husain, M. Roukes, *Appl. Phys. Lett.* **2005**, *86*, 223105.
- [64] J. Lee, Z. Wang, K. He, R. Yang, J. Shan, P. X.-L. Feng, *Sci. Adv.* **2018**, *4*, eaao6653.
- [65] J. Zhu, B. Xu, F. Xiao, Y. Liang, C. Jiao, J. Li, Q. Deng, S. Wu, T. Wen, S. Pei, *Nano Lett.* **2022**.
- [66] S. Truax, S.-W. Lee, M. Muoth, C. Hierold, *Nano Lett.* **2014**, *14*, 6092.
- [67] X. Wei, Q. Chen, S. Xu, L. Peng, J. Zuo, *Adv. Funct. Mater.* **2009**, *19*, 1753.
- [68] J. Zhou, N. Moldovan, L. Stan, H. Cai, D. A. Czaplewski, D. López, *Nano Lett.* **2020**, *20*, 5693.
- [69] P. Guzman, T. Dinh, H.-P. Phan, A. P. Joy, A. Qamar, B. Bahreyni, Y. Zhu, M. Rais-Zadeh, H. Li, N.-T. Nguyen, *Mater. Des.* **2020**, *194*, 108922.
- [70] I.-B. Baek, S. Byun, B. K. Lee, J.-H. Ryu, Y. Kim, Y. S. Yoon, W. I. Jang, S. Lee, H. Y. Yu, *Sci. Rep.* **2017**, *7*, 1.
- [71] A. R. Kermany, G. Brawley, N. Mishra, E. Sheridan, W. P. Bowen, F. Iacopi, *Appl. Phys. Lett.* **2014**, *104*, 081901.
- [72] S. Manzeli, D. Dumcenco, G. M. Marega, A. Kis, *Nat. Commun.* **2019**, *10*, 1.
- [73] G. Mu, N. Snell, C. Zhang, X. Xie, R. Tahvildari, A. Weck, M. Godin, R. St-Gelais, *J. Microelectromech. Syst.* **2022**.
- [74] A. Chiout, C. Brochard-Richard, L. Marty, N. Bendiab, M.-Q. Zhao, A. Johnson, F. Oehler, A. Ouerghi, J. Chaste, *npj 2D Mater. Appl.* **2023**, *7*, 1.
- [75] N. Krakover, B. R. Ilic, S. Krylov, *J. Micromech. Microeng.* **2022**, *32*, 054001.
- [76] G. A. Steele, A. K. Hüttel, B. Witkamp, M. Poot, H. B. Meerwaldt, L. P. Kouwenhoven, H. S. van der Zant, *Science* **2009**, *325*, 1103.
- [77] J. Kwon, J. Choi, K. Kim, J. Sim, J. Kim, J. Kim, *IEEE Trans. Magn.* **2009**, *45*, 2332.
- [78] H. Cho, M.-F. Yu, A. F. Vakakis, L. A. Bergman, D. M. McFarland, *Nano Lett.* **2010**, *10*, 1793.
- [79] F. Ye, J. Lee, P. X.-L. Feng, *Nano Lett.* **2018**, *18*, 1678.
- [80] J. Chaste, M. Sledzinska, M. Zdrojek, J. Moser, A. Bachtold, *Appl. Phys. Lett.* **2011**, *99*, 213502.
- [81] Z. Ning, T. Shi, M. Fu, Y. Guo, X. Wei, S. Gao, Q. Chen, *Nano Lett.* **2014**, *14*, 1221.
- [82] M. Dilena, M. F. Dell'Oste, J. Fernández-Sáez, A. Morassi, R. Zaera, *Mechanical Systems and Signal Processing* **2019**, *116*, 261.
- [83] A. W. McFarland, M. A. Poggi, M. J. Doyle, L. A. Bottomley, J. S. Colton, *Appl. Phys. Lett.* **2005**, *87*, 053505.
- [84] X. Shen, Z. Lv, K. Ichikawa, H. Sun, L. Sang, Z. Huang, Y. Koide, S. Koizumi, M. Liao, *Ultramicroscopy* **2022**, *234*, 113464.
- [85] M. J. Burek, D. Ramos, P. Patel, I. W. Frank, M. Lončar, *Appl. Phys. Lett.* **2013**, *103*, 131904.
- [86] P. Singh, R. Yadava, *IEEE Sens. J.* **2018**, *18*, 7529.
- [87] J. Chaste, A. Eichler, J. Moser, G. Ceballos, R. Rurali, A. Bachtold, *Nat. Nanotechnol.* **2012**, *7*, 301.
- [88] C. Lee, X. Wei, J. W. Kysar, J. Hone, *Science* **2008**, *321*, 385.
- [89] T. Mohiuddin, A. Lombardo, R. Nair, A. Bonetti, G. Savini, R. Jalil, N. Bonini, D. Basko, C. Galiotis, N. Marzari, *Phys. Rev. B* **2009**, *79*, 205433.
- [90] D. Tan, X. Cao, J. Huang, Y. Peng, L. Zeng, Q. Guo, N. Sun, S. Bi, R. Ji, C. Jiang, *Adv. Sci.* **2022**, 2201443.
- [91] D. Tan, N. Sun, L. Chen, J. Bu, C. Jiang, *ACS Appl. Nano Mater.* **2021**, *5*, 1034.
- [92] J. Lee, Z. Wang, K. He, J. Shan, P. X.-L. Feng, *ACS Nano* **2013**, *7*, 6086.
- [93] J. Molina, J. E. Escobar, D. Ramos, E. Gil-Santos, J. J. Ruz, J. Tamayo, Á. S. Paulo, M. Calleja, *Nano Lett.* **2021**, *21*, 6617.
- [94] C. Jiang, C. Tang, J. Song, *Nano Lett.* **2015**, *15*, 1128.
- [95] M. Li, H. X. Tang, M. L. Roukes, *Nat. Nanotechnol.* **2007**, *2*, 114.
- [96] Y.-T. Yang, C. Callegari, X. Feng, K. L. Ekinci, M. L. Roukes, *Nano Lett.* **2006**, *6*, 583.
- [97] X. Feng, R. He, P. Yang, M. Roukes, *Nano Lett.* **2007**, *7*, 1953.
- [98] R. He, X. Feng, M. Roukes, P. Yang, *Nano Lett.* **2008**, *8*, 1756.

- [99] D. Presnov, S. Kafanov, A. A. Dorofeev, I. V. Bozhev, A. S. Trifonov, Y. A. Pashkin, V. A. Krupenin, *JETP Lett.* **2018**, *108*, 492.
- [100] S. C. Jun, X. Huang, M. Manolidis, C. Zorman, M. Mehregany, J. Hone, *Nanotechnology* **2006**, *17*, 1506.
- [101] I. Bargatin, I. Kozinsky, M. Roukes, *Appl. Phys. Lett.* **2007**, *90*, 093116.
- [102] J. M. Gray, K. A. Bertness, N. A. Sanford, C. T. Rogers, *Appl. Phys. Lett.* **2012**, *101*, 233115.
- [103] L. Sang, M. Liao, X. Yang, H. Sun, J. Zhang, M. Sumiya, B. Shen, *Sci. Technol. Adv. Mater.* **2020**, *21*, 515.
- [104] H. Sun, L. Sang, X. Shen, X. Yang, T. Li, J. You, B. Shen, M. Liao, *J. Appl. Phys.* **2022**, *131*, 054502.
- [105] R. Voelkel, U. Vogler, A. Bich, P. Pernet, K. J. Weible, M. Hornung, R. Zoberbier, E. Cullmann, L. Stuerzebecher, T. Harzendorf, *Opt. Express* **2010**, *18*, 20968.
- [106] S. D. Gittard, R. J. Narayan, *Expert Rev. Med. Devices* **2010**, *7*, 343.
- [107] M. Boscardin, S. Ferrari, F. Ficorella, A. Lai, R. Mendicino, M. Meschini, S. Ronchin, M. A. A. Samy, G.-F. D. Betta, *Frontiers in Physics* **2021**, *8*, 625275.
- [108] P. Guzman, T. Dinh, A. Qamar, J. Lee, X. Zheng, P. Feng, M. Rais-Zadeh, H.-P. Phan, T. Nguyen, A. R. M. Foisal, *Sens. Actuators, A* **2022**, *343*, 113678.
- [109] H. Hu, H. Cho, S. Somnath, A. F. Vakakis, W. P. King, *Nanotechnology* **2014**, *25*, 275301.
- [110] T. A. Pham, A. Qamar, T. Dinh, M. K. Masud, M. Rais-Zadeh, D. G. Senesky, Y. Yamauchi, N. T. Nguyen, H. P. Phan, *Adv. Sci.* **2020**, *7*, 2001294.
- [111] K. Ekinici, M. Roukes, *Rev. Sci. Instrum.* **2005**, *76*, 061101.
- [112] B. Witkamp, M. Poot, H. S. van der Zant, *Nano Lett.* **2006**, *6*, 2904.
- [113] R. Yang, X. Zheng, Z. Wang, C. J. Miller, P. X.-L. Feng, *J. Vac. Sci. Technol., B: Nanotechnol. Microelectron.: Mater., Process., Meas., Phenom.* **2014**, *32*, 061203.
- [114] E. Kukovitsky, S. L'vov, N. Sainov, *Chem. Phys. Lett.* **2000**, *317*, 65.
- [115] X. M. H. Huang, R. Caldwell, L. Huang, S. C. Jun, M. Huang, M. Y. Sfeir, S. P. O'Brien, J. Hone, *Nano Lett.* **2005**, *5*, 1515.
- [116] A. K. Huttel, G. A. Steele, B. Witkamp, M. Poot, L. P. Kouwenhoven, H. S. van der Zant, *Nano Lett.* **2009**, *9*, 2547.
- [117] S. Grall, I. Dufour, V. Aubry, H. Debéda, *Smart Mater. Struct.* **2019**, *28*, 105055.
- [118] Y. Tadokoro, K. Funayama, K. Kawano, A. Miura, J. Hirotoni, Y. Ohno, H. Tanaka, *Microsyst. Nanoeng.* **2023**, *9*, 32.
- [119] O. Cooper, H.-P. Phan, T. Fitzpatrick, T. Dinh, H. Huang, N.-T. Nguyen, J. Tiralongo, *Biosens. Bioelectron.* **2022**, *205*, 114088.
- [120] X.-Q. Zheng, J. Lee, P. X.-L. Feng, *Microsyst. Nanoeng.* **2017**, *3*, 1.
- [121] J. Doster, S. Hönl, H. Lorenz, P. Paulitschke, E. M. Weig, *Nat. Commun.* **2019**, *10*, 1.
- [122] B. Svilčić, E. Mastropaolo, R. Cheung, *Sens. Actuators, A* **2015**, *226*, 149.
- [123] A. Sanz-Jiménez, J. J. Ruz, E. Gil-Santos, O. Malvar, S. García-López, P. M. Kosaka, Á. Cano, M. Calleja, J. Tamayo, *ACS Sens.* **2023**.
- [124] P. Weber, J. Guttinger, I. Tsioutsios, D. E. Chang, A. Bachtold, *Nano Lett.* **2014**, *14*, 2854.
- [125] M. J. Beryhi, A. Beccari, S. A. Fedorov, A. H. Ghadimi, R. Schilling, D. J. Wilson, N. J. Engelsen, T. J. Kippenberg, *Nano Lett.* **2019**, *19*, 2329.
- [126] Y. Tsaturyan, A. Barg, E. S. Polzik, A. Schliesser, *Nat. Nanotechnol.* **2017**, *12*, 776.
- [127] M. J. Beryhi, A. Beccari, R. Groth, S. A. Fedorov, A. Arabmoheghi, T. J. Kippenberg, N. J. Engelsen, *Nat. Commun.* **2022**, *13*, 1.
- [128] P. Sadeghi, M. Tanzer, S. L. Christensen, S. Schmid, *J. Appl. Phys.* **2019**, *126*, 165108.
- [129] Y. Fu, L. Li, Y. Hu, *Journal of Thermal Stresses* **2019**, *42*, 341.
- [130] W. Gao, F. Wang, O. Sigmund, *Computer Methods in Applied Mechanics and Engineering* **2020**, *361*, 112692.
- [131] Y. Fu, L. Li, K. Duan, Y. Hu, *Thin-Walled Structures* **2021**, *166*, 108104.
- [132] H.-P. Phan, T. Dinh, T. Kozeki, T.-K. Nguyen, A. Qamar, T. Namazu, N.-T. Nguyen, D. V. Dao, *Appl. Phys. Lett.* **2016**, *109*, 123502.
- [133] A. H. Ghadimi, S. A. Fedorov, N. J. Engelsen, M. J. Beryhi, R. Schilling, D. J. Wilson, T. J. Kippenberg, *Science* **2018**, *360*, 764.
- [134] F. Iacopi, G. Walker, L. Wang, L. Malesys, S. Ma, B. V. Cunniff, A. Iacopi, *Appl. Phys. Lett.* **2013**, *102*, 011908.
- [135] A. H. Ghadimi, D. J. Wilson, T. J. Kippenberg, *Nano Lett.* **2017**, *17*, 3501.
- [136] S. A. Fedorov, N. J. Engelsen, A. H. Ghadimi, M. J. Beryhi, R. Schilling, D. J. Wilson, T. J. Kippenberg, *Phys. Rev. B* **2019**, *99*, 054107.
- [137] P.-L. Yu, K. Cicak, N. Kampel, Y. Tsaturyan, T. Purdy, R. Simmonds, C. Regal, *Appl. Phys. Lett.* **2014**, *104*, 023510.
- [138] N. P. Mauranyapin, A. Terrasson, W. P. Bowen, *Advanced Quantum Technologies* **2022**, *5*, 2100139.
- [139] J. N. Kirchoff, Y. Yu, G. Antheaume, G. Gordeev, D. Yagodkin, P. Elliott, D. B. de Araújo, S. Sharma, S. Reich, K. I. Bolotin, *Nano Lett.* **2022**.
- [140] M. Šiškins, M. Lee, S. Mañas-Valero, E. Coronado, Y. M. Blanter, H. S. van der Zant, P. G. Steeneken, *Nat. Commun.* **2020**, *11*, 1.
- [141] M. Šiškins, S. Kurdi, M. Lee, B. J. Slotboom, W. Xing, S. Mañas-Valero, E. Coronado, S. Jia, W. Han, T. van der Sar, *npj 2D Materials and Applications* **2022**, *6*, 1.
- [142] I. E. Rostań, A. Japaridze, P. G. Steeneken, C. Dekker, F. Alijani, *Nat. Nanotechnol.* **2022**, *1*.
- [143] G. Longo, L. Alonso-Sarduy, L. M. Rio, A. Bizzini, A. Trampuz, J. Notz, G. Dietler, S. Kasas, *Nat. Nanotechnol.* **2013**, *8*, 522.
- [144] A. Sanz-Jiménez, O. Malvar, J. J. Ruz, S. García-López, P. M. Kosaka, E. Gil-Santos, Á. Cano, D. Papanastasiou, D. Kounadis, E. Panagiotopoulos, 2023 IEEE 36th International Conference on Micro Electro Mechanical Systems (MEMS), IEEE, **2023**, 444.
- [145] K. Jensen, K. Kim, A. Zettl, *Nat. Nanotechnol.* **2008**, *3*, 533.
- [146] C.-H. Weng, G. Pillai, S.-S. Li, *IEEE Sens. J.* **2020**, *20* 7001.
- [147] A. A. Zope, J.-H. Chang, T.-Y. Liu, S.-S. Li, *IEEE Trans. Electron Devices* **2020**, *67*, 1183.
- [148] J. M. L. Miller, H. Zhu, D. B. Heinz, Y. Chen, I. B. Flader, D. D. Shin, J. E.-Y. Lee, T. W. Kenny, *Phys. Rev. Appl.* **2018**, *10*, 044055.
- [149] C.-C. Chu, S. Dey, T.-Y. Liu, C.-C. Chen, S.-S. Li, *J. Microelectromech. Syst.* **2017**, *27*, 59.
- [150] M. S. Hanay, S. I. Kelber, C. D. O'Connell, P. Mulvaney, J. E. Sader, M. L. Roukes, *Nat. Nanotechnol.* **2015**, *10*, 339.
- [151] N. V. Lavrik, P. G. Datskos, *Appl. Phys. Lett.* **2003**, *82*, 2697.
- [152] X. Han, Q. Mao, L. Zhao, X. Li, L. Wang, P. Yang, D. Lu, Y. Wang, X. Yan, S. Wang, *Microsyst. Nanoeng.* **2020**, *6*, 1.
- [153] K. Duan, L. Li, Y. Hu, X. Wang, *Sci. Rep.* **2017**, *7*, 14012.
- [154] M. S. Hanay, S. Kelber, A. Naik, D. Chi, S. Hentz, E. Bullard, E. Colinet, L. Duraffourg, M. Roukes, *Nat. Nanotechnol.* **2012**, *7*, 602.
- [155] E. Sage, M. Sansa, S. Fostner, M. Defoort, M. Gély, A. K. Naik, R. Morel, L. Duraffourg, M. L. Roukes, T. Alava, *Nat. Commun.* **2018**, *9*, 1.
- [156] S. Dominguez-Medina, S. Fostner, M. Defoort, M. Sansa, A.-K. Stark, M. A. Halim, E. Vernhes, M. Gely, G. Jourdan, T. Alava, *Science* **2018**, *362*, 918.
- [157] D. Ramos Vega, E. Gil-Santos, V. Pini, J. M. Llorens Montolio, M. Fernández-Regúlez, Á. S. Paulo, M. Calleja, F. J. Tamayo de Miguel, **2012**.
- [158] B.-D. Chan, K. Icoz, W. Huang, C.-L. Chang, C. A. Savran, *Lab Chip* **2014**, *14*, 4188.
- [159] M. Krieg, G. Fläschner, D. Alsteens, B. M. Gaub, W. H. Roos, G. J. Wuite, H. E. Gaub, C. Gerber, Y. F. Dufrière, D. J. Müller, *Nature Reviews Physics* **2019**, *1*, 41.
- [160] F. Braakman, M. Poggio, *Nanotechnology* **2019**, *30*, 332001.

- [161] F. Fogliano, B. Besga, A. Reigue, L. M. de Lépinay, P. Heringlake, C. Gouriou, E. Eyraud, W. Wernsdorfer, B. Pigeau, O. Arcizet, *arXiv preprint* **2020**.
- [162] J. Moser, J. Güttinger, A. Eichler, M. J. Esplandiú, D. Liu, M. Dykman, A. Bachtold, *Nat. Nanotechnol.* **2013**, *8*, 493.
- [163] P. Weber, J. Güttinger, A. Noury, J. Vergara-Cruz, A. Bachtold, *Nat. Commun.* **2016**, *7*, 1.
- [164] L. M. de Lépinay, B. Pigeau, B. Besga, P. Vincent, P. Poncharal, O. Arcizet, *Nat. Nanotechnol.* **2017**, *12*, 156.
- [165] M. Héritier, A. Eichler, Y. Pan, U. Grob, I. Shorubalko, M. D. Krass, Y. Tao, C. L. Degen, *Nano Lett.* **2018**, *18*, 1814.
- [166] J. Moser, A. Eichler, J. Güttinger, M. I. Dykman, A. Bachtold, *Nat. Nanotechnol.* **2014**, *9*, 1007.
- [167] J. M. Nichol, E. R. Hemesath, L. J. Lauhon, R. Budakian, *Phys. Rev. B* **2012**, *85*, 054414.
- [168] J. Gieseler, L. Novotny, R. Quidant, *Nat. Phys.* **2013**, *9*, 806.
- [169] J. S. Bunch, A. M. Van Der Zande, S. S. Verbridge, I. W. Frank, D. M. Tanenbaum, J. M. Parpia, H. G. Craighead, P. L. McEuen, *Science* **2007**, *315*, 490.
- [170] K. Wojciechowski, B. Boser, A. Pisano, *SENSORS* **2005**, *4*.
- [171] K. E. Wojciechowski, B. E. Boser, A. P. Pisano, *Technical Digest* **2004**, 841.
- [172] R. G. Azevedo, D. G. Jones, A. V. Jog, B. Jamshidi, D. R. Myers, L. Chen, X.-a. Fu, M. Mehregany, M. B. Wijesundara, A. P. Pisano, *IEEE Sens. J.* **2007**, *7*, 568.
- [173] S. Kon, R. Horowitz, *IEEE Sens. J.* **2008**, *8*, 2027.
- [174] M. Schlögl, J. Weissenbach, M. Schneider, U. Schmid, *Sens. Actuators, A* **2023**, *349*, 114067.
- [175] M. Aikele, K. Bauer, W. Ficker, F. Neubauer, U. Prechtel, J. Schalk, H. Seidel, *Sens. Actuators, A* **2001**, *92*, 161.
- [176] J. Věříš, *Sens. Actuators, A* **1996**, *57*, 179.
- [177] C. J. Welham, J. W. Gardner, J. Greenwood, *Sens. Actuators, A* **1996**, *52*, 86.
- [178] D. Burns, J. Zook, R. Horning, W. Herb, H. Guckel, *Sens. Actuators, A* **1995**, *48*, 179.
- [179] J. Lee, P. X.-L. Feng, *IEEE International Frequency Control Symposium (FCS)* **2014**, *1*.
- [180] X. Du, L. Wang, A. Li, L. Wang, D. Sun, *J. Microelectromech. Syst.* **2016**, *26*, 235.
- [181] Y. Li, J. Wang, Z. Luo, D. Chen, J. Chen, *Sensors* **2015**, *15*, 10048.
- [182] Y. Lu, P. Yan, C. Xiang, D. Chen, J. Wang, B. Xie, J. Chen, *Sensors* **2019**, *19*, 2272.
- [183] X. Du, Y. Liu, A. Li, Z. Zhou, D. Sun, L. Wang, *Sensors* **2016**, *16*, 158.
- [184] S. Ren, W. Yuan, D. Qiao, J. Deng, X. Sun, *Sensors* **2013**, *13*, 17006.
- [185] C. J. Welham, J. Greenwood, M. M. Bertoli, *Sens. Actuators, A* **1999**, *76*, 298.
- [186] N. Yazdi, F. Ayazi, K. Najafi, *Proceedings of the IEEE* **1998**, *86*, 1640.
- [187] T. A. Roessig, R. T. Howe, A. P. Pisano, J. H. Smith, *Proceedings of International Solid State Sensors and Actuators Conference (Transducers' 97)*, IEEE, **1997**, 859.
- [188] A. G. Krause, M. Winger, T. D. Blasius, Q. Lin, O. Painter, *Nat. Photonics* **2012**, *6*, 768.
- [189] L. Xu, Y. Qi, Z. Jiang, X. Wei, *Microsystems & nanoengineering* **2022**, *8*, 1.
- [190] A. Eichler, *arXiv preprint* **2022**.
- [191] M. Seo, E. Yang, D. H. Shin, Y. Je, C. Joo, K. Lee, S. W. Lee, *ACS Applied Electronic Materials* **2022**.
- [192] S. Tepsic, G. Gruber, C. Möller, C. Magén, P. Belardinelli, E. R. Hernández, F. Alijani, P. Verlot, A. Bachtold, *Phys. Rev. Lett.* **2021**, *126*, 175502.
- [193] T. Larsen, S. Schmid, L. Grönberg, A. Niskanen, J. Hassel, S. Dohn, A. Boisen, *Appl. Phys. Lett.* **2011**, *98*, 121901.
- [194] B. Kim, M. A. Hopcroft, R. N. Candler, C. M. Jha, M. Agarwal, R. Melamud, S. A. Chandorkar, G. Yama, T. W. Kenny, *J. Microelectromech. Syst.* **2008**, *17*, 755.
- [195] J. Verd, M. Sansa, A. Uranga, F. Perez-Murano, J. Segura, N. Barniol, *Lab Chip* **2011**, *11*, 2670.
- [196] J. Verd, M. Sansa, A. Uranga, C. Pey, G. Abadal, F. Perez-Murano, N. Barniol, *Actuators and Microsystems Conference, IEEE*, **2009**, 2429–2432.
- [197] A. Cagliani, V. Pini, J. Tamayo, M. Calleja, Z. J. Davis, *Sens. Actuators, B* **2014**, *202*, 339.
- [198] W. Sui, H. Wang, J. Lee, A. Qamar, M. Rais-Zadeh, P. X. L. Feng, *Adv. Funct. Mater.* **2022**, *32*, 2202204.
- [199] U. Adiyen, T. Larsen, J. J. Zárate, L. G. Villanueva, H. Shea, *Nat. Commun.* **2019**, *10*, 1.
- [200] R. Yang, Z. Wang, P. X.-L. Feng, 2015 Joint Conference of the IEEE International Frequency Control Symposium & the European Frequency and Time Forum, IEEE, **2015**, 198.
- [201] M. Wang, R. Zhang, R. Ilic, V. Aksyuk, Y. Liu, *Nano Lett.* **2020**, *20*, 3050.
- [202] Z. Qian, Y. Hui, F. Liu, S. Kang, S. Kar, M. Rinaldi, *Microsyst. Nanoeng.* **2016**, *2*, 1.
- [203] G. Piazza, P. J. Stephanou, A. P. Pisano, *J. Microelectromech. Syst.* **2006**, *15*, 1406.
- [204] A. Ansari, M. Rais-Zadeh, *IEEE Electron Device Lett.* **2014**, *35*, 1127.
- [205] M. B. Pisani, K. Ren, P. Kao, S. Tadigadapa, *J. Microelectromech. Syst.* **2011**, *20*, 288.
- [206] R. Lu, S. Gong, *Transducers-2015 18th International Conference on Solid-State Sensors, Actuators and Microsystems (TRANSDUCERS)*, IEEE, **2015**, 1993.
- [207] F. Lu, J. Lee, A. Jiang, S. Jung, M. A. Belkin, *Nat. Commun.* **2016**, *7*, 1.
- [208] Y. Hui, J. S. Gomez-Diaz, Z. Qian, A. Alu, M. Rinaldi, *Nat. Commun.* **2016**, *7*, 1.
- [209] T. Inoue, Y. Mochizuki, K. Takei, T. Arie, S. Akita, *2D Mater.* **2018**, *5*, 045022.
- [210] S. Saxena, T. B. Ashagre, D. Rakshit, S. Das, V. R. Rao, 2023 IEEE Applied Sensing Conference (APSCON), IEEE, **2023**, 1–3.
- [211] M. B. Coskun, M. Rais-Zadeh, 5th IEEE Electron Devices Technology & Manufacturing Conference (EDTM), IEEE, **2021**, 1–3.
- [212] M. Kucera, E. Wistrela, G. Pfusterschmied, V. Ruiz-Díez, T. Manzaneeque, J. Hernando-García, J. L. Sánchez-Rojas, A. Jachimowicz, J. Schalko, A. Bittner, *Sens. Actuators, B* **2014**, *200*, 235.
- [213] J. Toledo, T. Manzaneeque, J. Hernando-García, J. Vázquez, A. Ababneh, H. Seidel, M. Lapuerta, J. L. Sánchez-Rojas, *Microsystem technologies* **2014**, *20*, 945.
- [214] J. Yang, J. Xu, W. Wu, M. Bertke, H. S. Wasisto, E. Peiner, *Proc. Eng.* **2016**, *168*, 1114.
- [215] R. Nuryadi, L. Aprilia, M. Hosoda, M. A. Barique, A. Udhiarto, D. Hartanto, M. B. Setiawan, Y. Neo, H. Mimura, *Sensors* **2020**, *20*, 2013.
- [216] K. Mistry, V. H. Nguyen, M. Arabi, K. H. Ibrahim, H. Asgarimoghaddam, M. Yavuz, D. Muñoz-Rojas, E. Abdel-Rahman, K. P. Musselman, *Nano Lett.* **2022**, *22*, 3196.
- [217] S. J. Martin, V. E. Granstaff, G. C. Frye, *Anal. Chem.* **1991**, *63*, 2272.
- [218] M. K. Ghatkesar, T. Braun, V. Barwich, J.-P. Ramseyer, C. Gerber, M. Hegner, H. P. Lang, *Appl. Phys. Lett.* **2008**, *92*, 043106.
- [219] J. Pettine, M. Patrascu, D. Karabacak, M. Vandecasteele, V. Petrescu, S. Brongersma, M. Crego-Calama, C. Van Hoof, *Sens. Actuators, A* **2013**, *189*, 496.
- [220] T. Manzaneeque, V. Ruiz-Díez, J. Hernando-García, E. Wistrela, M. Kucera, U. Schmid, J. L. Sánchez-Rojas, *Sens. Actuators, A* **2014**, *220*, 305.

- [221] J. Toledo, V. Ruiz-Díez, G. Pfusterschmied, U. Schmid, J. Sánchez-Rojas, *Sens. Actuators, B* **2018**, 254, 291.
- [222] L. Huang, W. Li, G. Luo, D. Lu, L. Zhao, P. Yang, X. Wang, J. Wang, Q. Lin, Z. Jiang, *Microsystems & nanoengineering* **2022**, 8, 1.
- [223] A. Ali, J.-Y. Lee, *Sens. Actuators, A* **2016**, 241, 216.
- [224] I. Dufour, E. Lemaire, B. Caillard, H. Debéda, C. Lucat, S. M. Heinrich, F. Josse, O. Brand, *Sens. Actuators, B* **2014**, 192, 664.
- [225] J. H. Seo, O. Brand, *J. Microelectromech. Syst.* **2008**, 17, 483.
- [226] C. Riesch, E. K. Reichel, A. Jachimowicz, J. Schalko, P. Hudek, B. Jakoby, F. Keplinger, *J. Micromech. Microeng.* **2009**, 19, 075010.
- [227] J. Lee, Y. Zhu, A. Seshia, *J. Micromech. Microeng.* **2008**, 18, 025033.
- [228] A. N. Cleland, M. L. Roukes, *Nature* **1998**, 392, 160.
- [229] H. Krömmmer, A. Erbe, A. Tilke, S. Manus, R. Blick, *EPL (Europhysics Letters)* **2000**, 50, 101.
- [230] A. Dash, S. K. More, N. Arora, A. Naik, *Appl. Phys. Lett.* **2021**, 118, 053105.



Toan Dinh is an Associate Professor in the School of Engineering, University of Southern Queensland, Australia. His research interests include micro/nano-electromechanical systems (MEMS/NEMS), physics of semiconductors, sensors for harsh environments, soft robotics, and advanced materials for healthcare and wearable applications.